

Observations, Modeling and Theory of Debris Disks

Brenda C. Matthews

National Research Council of Canada – Herzberg Astronomy & Astrophysics

Alexander V. Krivov

Friedrich-Schiller-Universität Jena

Mark C. Wyatt

University of Cambridge

Geoffrey Bryden

Jet Propulsion Laboratory

Carlos Eiroa

Universidad Autónoma de Madrid

Main sequence stars, like the Sun, are often found to be orbited by circumstellar material that can be categorized into two groups, planets and debris. The latter is made up of asteroids and comets, as well as the dust and gas derived from them, which makes debris disks observable in thermal emission or scattered light. These disks may persist over Gyrs through steady-state evolution and/or may also experience sporadic stirring and major collisional breakups, rendering them atypically bright for brief periods of time. Most interestingly, they provide direct evidence that the physical processes (whatever they may be) that act to build large oligarchs from micron-sized dust grains in protoplanetary disks have been successful in a given system, at least to the extent of building up a significant planetesimal population comparable to that seen in the Solar System’s asteroid and Kuiper belts. Such systems are prime candidates to host even larger planetary bodies as well. The recent growth in interest in debris disks has been driven by observational work that has provided statistics, resolved images, detection of gas in debris disks, and discoveries of new classes of objects. The interpretation of this vast and expanding dataset has necessitated significant advances in debris disk theory, notably in the physics of dust produced in collisional cascades and in the interaction of debris with planets. Application of this theory has led to the realization that such observations provide a powerful diagnostic that can be used not only to refine our understanding of debris disk physics, but also to challenge our understanding of how planetary systems form and evolve.

1. INTRODUCTION

Our evolving understanding of debris disks through the PP series was succinctly summarized by *Meyer et al.* (2007), emphasizing the important role they play in studies of planetary systems and stressing the need to resolve disks to break the degeneracies inherent in spectral energy distribution (SED) modeling, setting well the stage for the near-decade of debris disk science that has come and gone since. The *Spitzer Space Telescope*’s debris disk surveys are complete and now in the literature, and these are augmented significantly by those of the *Herschel Space Observatory*, which will have a lasting legacy owing to its resolving power and wavelength coverage. In parallel, there have been similar or even superior resolving power breakthroughs at wavelengths from the near-IR (e.g., CHARA, VLTI, LBTI) to (sub)millimeter (i.e., ALMA, SMA and CARMA) on the ground.

In this chapter we focus exclusively on debris disks, circumstellar dust (and potentially gas) disks created through destructive processes acting on larger, unseen planetesimals within the disk systems. A key diagnostic of a debris disk is the low fractional luminosity of the dust; even the brightest debris disks are ~ 100 times fainter than protoplanetary disks, and most are ~ 100 times fainter still. Our goal for this chapter remains the same as previous PP proceedings authors: to understand the evolution of planetary systems through observations of the circumstellar dust and gas that surrounds many of these systems throughout their lifetime using physical models.

Our chapter is divided as follows. In § 2, we discuss how disks are detected and characterized, highlighting results from recent surveys followed by § 3 on the origin of dust in collisional cascades. We then discuss the birth and evolution of debris disks in § 4. In § 5 we present the signifi-

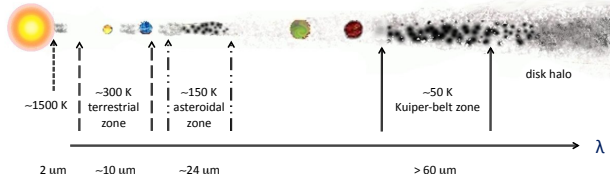


Fig. 1.— Locations of dust emission observed in debris disks and the typical temperatures observed at those locations, and the **primary** observing wavelengths at which the dust is detected. (Figure credit: K. Su.)

cant advances in debris disk imaging, followed by a section on the origin of structure through perturbations (§ 6). Finally we highlight observations and origin scenarios of hot dust (§ 7) and gas (§ 8) in debris disks. We summarize our chapter and provide an outlook to the future in § 9.

2. DETECTION AND DISTRIBUTION OF DUST

Observations of debris disks help not only to study the properties of individual disks, but also to ascertain their incidence and their correlation with stellar properties – e.g., age, spectral type, metallicity, stellar and/or planetary companions. Therefore, their study is imperative to understand the diversity of planetary system architectures and to thereby place the Solar System’s debris disk, primarily composed of warm dust in the terrestrial planet zone, the asteroid belt (0.5 - 3 AU) and cold dust and planetesimals in the Edgeworth-Kuiper belt (EKB), in context.

While at optical and near-infrared (IR) wavelengths, scattered light from dust grains highlights regions of disks where small grains dominate, dust is most effectively traced by its thermal emission. Typically, evidence of a disk comes from “excess” IR emission detected above the level of the stellar photosphere. Figure 1 highlights the dust temperatures that are probed by different observing wavelength regimes. If a disk is comprised of multiple components at a range of distances from the star, then observations at different wavelengths can probe the different components, with shorter wavelengths probing closer in material, as illustrated for *IRAS*, *Spitzer* (MIPS) and *Herschel* (PACS) observing wavelengths by Figure 2.

The emerging picture is that disks commonly are comprised of multiple components as Figure 1 illustrates, but that does not mean that all components are necessarily present or detectable around all stars. For many disks, just one component, typically (but not always) that in the Kuiper belt zone, dominates the detected emission, and in such cases, observations over a range of wavelengths provide a probe of different dust grain sizes, with longer wavelengths probing larger grains. In addition, the comparison and complementarity of the different statistical studies are modulated by the different observational strategies and target properties, e.g., spectral type (see Fig. 2), and on distance according to the nature of the survey (sensitivity vs.

calibration-limited strategies, Wyatt 2008). Therefore, the flux contrast between the stellar photosphere and a potentially existing debris disk is mainly determined by the stellar temperature, modulated by the distance to the star (e.g., *Eiroa et al.* 2013). Both *Spitzer* and *Herschel* are well suited to carry out detailed statistical studies relating debris disk properties with stellar ones, i.e., to determine the frequency and characterize the nature of disks. Good summaries of the *Spitzer* results and statistics are given by Wyatt (2008) and *Krivov* (2010).

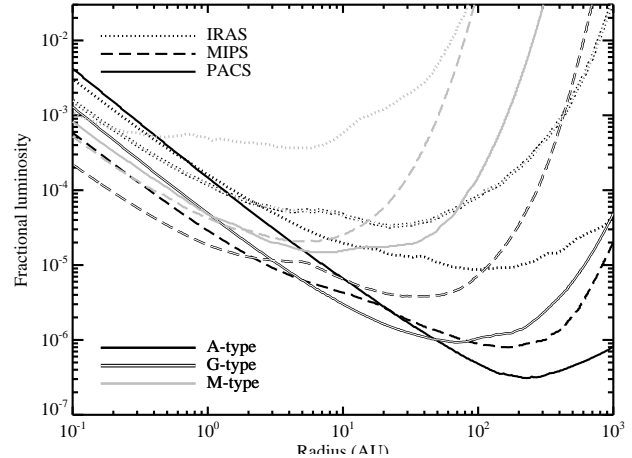


Fig. 2.— This plot shows, based on the DEBRIS survey data (*Matthews et al.* 2013b), the lines of fractional luminosity versus radius above which 25% of that sample could have been detected by *IRAS*, MIPS (24 & 70 μm) and PACS (100 & 160 μm), assuming each star to have a single temperature belt dominating its emission spectrum. The 25% level is comparable to the detection levels for many surveys given that DEBRIS is a survey of very nearby stars. (Figure credit: G. Kennedy.)

As sensitivity toward faint debris disks improves so too does sensitivity to extragalactic contamination. This is important because it impacts disk incidences, interpretation of structures, and the identification of new cold disk populations. The impact of background galaxy contamination has typically been a problem for surveys in the far-IR and submillimeter, but it has recently been identified as a major problem for *WISE* (*Wide-field Infrared Survey Explorer*) as well (*Kennedy and Wyatt* 2012).

In the following sections, we consider in turn our understanding of the different disk components as traced predominantly by observations in different wavelength regimes, but we stress that this does not represent a one-to-one correspondence with disk temperatures. For example, Figure 2 shows that MIPS/24 and PACS/100 are equally sensitive to dust at ~ 3 AU around G type stars (akin to our asteroid belt’s warm dust). As we discuss below, ALMA at (sub-)millimeter wavelengths now has the potential to detect even the warm dust components of disks, so *it is sensitivity as much as wavelength that is key to detecting dust*

over a range of temperature (or emitting radii).

2.1. Far-Infrared to Millimeter Observations

Many debris disks are detected only at long wavelengths ($\geq 60 \mu\text{m}$), corresponding to cold ($\lesssim 100 \text{ K}$) dust orbiting at 10s to 100s of AU. The debris disks detected with *IRAS* were Kuiper belt analogues seen around $\sim 15\%$ of main sequence stars (Aumann 1985). Rhee *et al.* (2007) have reanalyzed *IRAS* data and found the detection rate around nearby A stars to be 20%. In the past decade, *Spitzer* A stars (Rieke *et al.* 2005) and FEPS¹ (Meyer *et al.* 2006) surveys and *Herschel* DEBRIS² (Matthews *et al.* 2013b) and DUNES³ (Eiroa *et al.* 2013) surveys have measured the incidence of debris disks for spectral types A through M at 70 – 160 μm .

Keeping in mind the relative sensitivities of the various surveys (Fig. 2), the highest detection rates are measured for A stars: 33% and 25% at 70 μm (Su *et al.* 2006) and 100 μm (Thureau *et al.* 2013), respectively. For solar type stars (FGK), the FEPS survey detected disks around 10% of stars (Hillenbrand *et al.* 2008), while Trilling *et al.* (2008) measured a rate of 16% in the field, comparable to the rate detected by the DEBRIS survey (17%, Sibthorpe *et al.* 2013). The DUNES data yield an increase in the debris disk detection rate up to $\sim 20.2\%$ (in contrast to the *Spitzer* detection rate of $\sim 12.1\%$ for the same sample of FGK stars, Eiroa *et al.* 2013). Although there is an apparent decrease of excess rates from A to K spectral types, this appears to be largely an age effect (Su *et al.* 2006; Trilling *et al.* 2008). In this respect, Trilling *et al.* (2008) note that there is no trend among FGK stars of similar age in the FEPS survey and that the rates for AFGK stars are statistically indistinguishable, a result supported by DUNES data (Eiroa *et al.* 2013).

The amount of dust in debris disks is frequently quantified in terms of the fractional luminosity of the dust, $f_d \equiv L_d/L_*$, which is usually estimated assuming that the dust behaves as a pure or modified blackbody (see §3.5) emitter. f_d values are found in the range of $\sim 10^{-3}$ – 10^{-6} with a clear decrease towards older systems, although with a large dispersion at any given age (e.g., Siegler *et al.* 2007; Hillenbrand *et al.* 2008; Moór *et al.* 2011b). (The evolution of debris disks is discussed in more detail in § 4.4 below.) There is however no clear dependence of fractional luminosity on spectral type from late B to M, as shown in Figure 3, although the is high for all spectral types.

In spite of the remarkable contribution of *Spitzer*, its moderate sensitivity in terms of the dust fractional luminosity ($f_d \sim 10^{-5}$, Trilling *et al.* 2008) makes elusive the detection of debris disks with levels similar to the EKB ($\sim 10^{-7}$, Vitense *et al.* 2012). This constraint is somewhat mitigated by the *Herschel* surveys, which observed closer to the peak of the SEDs and therefore could detect fainter disks, e.g., DUNES observations of 133 FGK stars located

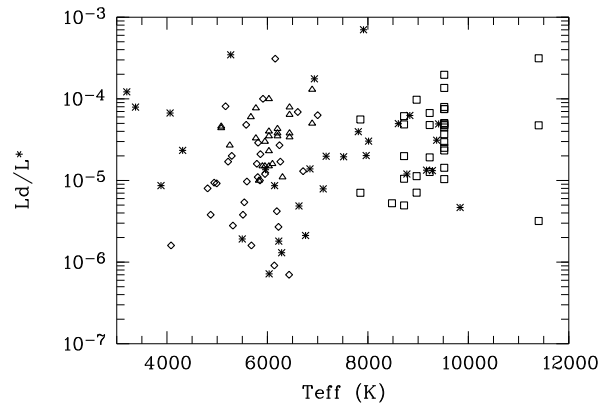


Fig. 3.— Fractional luminosity of dust versus effective stellar temperatures for main-sequence stars. Squares: A stars (Su *et al.* 2006); triangles: FGK stars (Trilling *et al.* 2008); diamonds: FGK stars (Eiroa *et al.* 2013); asterisks: AFGKM stars (Matthews *et al.* 2013b).

at distances less than 20 pc achieves an average sensitivity of $f_d \sim 10^{-6}$, although with a dependence on stellar flux (Eiroa *et al.* 2013). The DEBRIS survey, with flux-limited observations of 446 A through M nearby stars (Matthews *et al.* 2013b) has a median sensitivity of f_d of just 2×10^{-5} but a faintest detected disk of 7×10^{-7} , approaching the level of the EKB.

Based on Figures 2 and 3, increased sensitivity to fainter luminosity disks around A stars is expected in *Herschel* observations compared to *Spitzer*. Interestingly, DEBRIS data indicate there is not a significant number of detections of A star disks with fractional luminosities below the levels detected by *Spitzer* (Thureau *et al.* 2013), implying that there is not a significant fraction of undetected, colder (i.e., larger) disks around A stars awaiting discovery. In comparison, Figure 3 shows that, for the FGK stars, many disks of lower fractional luminosities have been detected by *Herschel* relative to *Spitzer*.

Detection of M star-hosted debris disks at rates comparable to those around more massive stars has proven difficult. There are several factors at play around M stars, e.g., wind-related grain removal processes which are more efficient than around more massive stars (e.g., Plavchan *et al.* 2005), which effectively removes small grains from the system, necessitating surveys at longer wavelengths to find comparable disks seen around earlier type stars (Matthews *et al.* 2007). That said, given their prevalence in the galaxy, the detection of protoplanetary disks at earlier phases of evolution (e.g., Andrews and Williams 2005), and the detection of extrasolar planets around a number of M dwarfs (e.g., Endl *et al.* 2008, and references therein), including multiple systems around GJ 876 (Rivera *et al.* 2005), GJ 581 (Udry *et al.* 2007) and GJ 676A (Anglada-Escudé and Tuomi 2012), we expect M stars to host planetesimal populations.

Figure 2 shows that existing observations of M stars

¹Formation and Evolution of Planetary Systems

²Disk Emission via a Bias-free Reconnaissance in the Infrared/Submillimetre

³Dust around NEarby Stars

are not sensitive to the same levels of fractional luminosity detectable toward earlier type stars. As might be expected, low detection rates around M stars are reported by many *Spitzer* studies, generally excepting only the very young systems (e.g., *Low et al.* 2005; *Gautier et al.* 2007; *Plavchan et al.* 2009; *Koerner et al.* 2010). One particular exception is the study of *Forbrich et al.* (2008) which detected excesses around eleven M stars in the 30 – 40 Myr NGC 2547 cluster at 24 μm , tracing warm material around 1 AU from the parent stars (close to the snow line). The M star disk incidence rate appears, in that cluster, to exceed that of G and K stars of the same age. The highest detection rate is quoted by *Lestrade et al.* (2006) using combined submillimeter studies to calculate an excess fraction of $13_{-8}^{+6}\%$ from 20–200 Myr targets, which is not markedly different from the field FGK incidence rates discussed above. *Avenhaus et al.* (2012) report no detections toward M stars in the *WISE* sample, which *Heng and Malik* (2013) attribute to the sensitivity of the *WISE* data to the ~ 1 AU region of the disk, where the planetesimals cannot persist for periods beyond 300 Myr, a prediction however at odds with the *WISE* disks reported around older, solar-type stars. Some disks are seen around older M star systems, however, such as the GJ 842.2 disk (*Lestrade et al.* 2006) and the 2 disks detected toward the 89 M stars surveyed for DEBRIS with *Herschel*, one of which is resolved around the old (2 – 8 Gyr) multi-planet host GJ 581 (*Lestrade et al.* 2012).

(Sub-)millimeter observations of debris disks typically trace the Rayleigh-Jeans tail of the outer cold dust (e.g., TWA 7, *Matthews et al.* 2007). They provide relevant constraints on the debris dust, e.g. measurement of the power-law exponent β of the opacity law and determination of the dust mass for sizes up to ~ 1 mm since emission at these wavelengths is optically thin. While most observations have concentrated on disks previously identified at other wavelengths, a few statistical surveys have been carried out, e.g., the JCMT survey by *Najita and Williams* (2005) and the CSO/IRAM survey of *Roccatagliata et al.* (2009). *Najita and Williams* (2005) detected 3 sources out of 13 nearby solar-mass stars, while 5 out of 27 FEPS sources older than 10 Myr were detected in the statistical analysis at 350 μm and/or 1.2 mm by *Roccatagliata et al.* (2009). An incidence rate of $\sim 60\%$ among a sample of 22 sources with previously known far-IR excesses was found in the APEX survey of *Nilsson et al.* (2010). We note, however, that this sample includes very young objects whose disks are still in a protostellar or transitional phase (see *Li et al.* 2014; *Dunham et al.* 2014; *Espaillet et al.* 2014, for more information on these disk phases). The SCUBA-2 Observations of Nearby Stars (SONS) Survey, currently underway, has achieved a detection rate of 40% for 850 μm detections of cold dust toward known disk hosts, including many not previously detected at submillimeter wavelengths (*Panić et al.* 2013).

2.2. Mid-Infrared Observations

Warm dust in the habitable zones of solar-type stars is of particular interest, both as a potential indicator of ongoing terrestrial planet formation and as a source of obscuration for future imaging of such planets. Mid-IR excess is difficult to detect, since the dust emission tends to be overwhelmed by the star. The zodiacal light in the Solar System, for example, would be less than 10^{-4} as bright as the Sun at 10 μm , if viewed from afar (*Kelsall et al.* 1998). Due to this limitation, photometric surveys for warm dust in the mid-IR are generally limited by their systematic floor, e.g., uncertainty in the instrument calibration and/or in the estimate for the stellar photosphere. Nevertheless, considerable progress has been made in detecting potential analogs to the Solar System’s warm dust around other stars, so-called exozodiacal dust.

Spitzer photometry and spectroscopy in the mid-IR yields detection rates that are a strong function of wavelength, spectral type and age. Only a few percent of mature solar-type stars exhibit mid-IR excess. For example, *Hillenbrand et al.* (2008) and *Dodson-Robinson et al.* (2011) find rates of $\sim 4\%$ at 24 μm in contrast to $\sim 16\%$ at 70 μm (*Trilling et al.* 2008), while *Lawler et al.* (2009) find a rate of $\sim 1\%$ in the range 8.5–12 μm versus $\sim 11.8\%$ in the 30–34 μm wavelength range.

Detection rates are higher for younger stars (e.g., in the Pleiades, *Gorlova et al.* 2006). In the 10–20 Myr old Sco-Cen association, the rates at 24 μm with *Spitzer* are comparable to those seen in the far-IR, i.e., 25% and 33% for B+A stars (*Chen et al.* 2012) and F+G stars (*Chen et al.* 2011), respectively. The rate for A stars of all ages is measured to be 32% at 24 μm (*Su et al.* 2006), comparable to the rate measured at 70 μm for the same stars. *Morales et al.* (2009, 2011) compiled a sample of 69 young (< 1 Gyr) nearby stars with 24 μm excess, most of which (50) occur around A-type stars. Within the FEPS sample, the rate of 24 μm excess is markedly higher (15%) for stars with ages < 300 Myr, compared to 2.7% at > 200 Myr (*Carpenter et al.* 2009).

Spectra or longer wavelength measurements not only help in constraining dust composition (§3.5), they also help in measuring the dust temperature, which can otherwise be ambiguous from just one or two photometric measurements (see Fig. 2). So while a *Spitzer*/IRS spectral survey of nearby solar-type stars found a relatively high rate of excess at 32 μm (*Lawler et al.* 2009), most of these detections were identified as the short-wavelength side of previously detected cold dust, not new detections of warm emission. Only two systems (1% of those observed) were detected at 10 μm – HD 69830 and η Crv – both identified as having dust at ~ 1 AU (*Beichman et al.* 2005a; *Wyatt et al.* 2005).

Additional systems with warm excess have been detected within the *IRAS*, *AKARI*, and *WISE* datasets which, as all-sky surveys, are well-suited toward identifying bright, rare objects. Examples include BD+20 307 (*Stencel and Backman* 1991; *Song et al.* 2005), HD 106797 (*Fujiwara et al.* 2009), and HD 15407 (*Melis et al.* 2010). The spec-

tra of these systems generally have strong silicate features at $10\ \mu\text{m}$, which provide useful constraints on the dust size and composition (see §3.5). These dust constraints, combined with the large amount of dust present and its short collisional lifetime, suggest that its origin lies in unusual collisional events (see §7). Most recently, *Kennedy and Wyatt* (2013) created a uniform catalog of bright warm-dust systems based on *WISE* $12\ \mu\text{m}$ excess. They find that such systems occur around $\sim 1\%$ of young stars (< 120 Myr), but are relatively rare for (\sim Gyr) old stars like BD+20 307 (10^{-4} frequency). While their survey only probes the bright end of the luminosity function, they extend their results down to fainter disks assuming a gradual collisional evolution, predicting that at least 10% of nearby stars will have sufficient dust in their habitable zones to pose problems for future efforts at direct imaging of exoEarths. On the other hand, *Melis et al.* (2012) report a rapid loss of IR excess for the young solar-type star TYC 8241 2652 1 – a factor of 30 reduction in less than 2 years. The dramatic change of this system remains unexplained.

Measurement of the typical amount of exozodiacal dust around nearby stars is an important step toward planning future imaging of Earth-like planets (*Roberge et al.* 2012). While it is possible to extrapolate from the brightest disks (e.g., *Lawler et al.* 2009; *Kennedy and Wyatt* 2013), the typical exozodi is still quite uncertain, where a *zodi* refers to the equivalent luminosity of a disk identical to the Solar System’s zodiacal cloud (*Roberge et al.* 2012). Future advancement in the detection of faint warm dust requires improved control over measurement systematics, as well as an understanding of the potential sources of confusion (e.g., *Kennedy and Wyatt* 2012). While spectroscopy is an improvement over photometry (calibration against ancillary photometry is not necessary; one can instead look for changes in slope within the spectrum itself), interferometry provides the best opportunity for robust detection of dust at levels much fainter than the star itself. A mid-IR survey by the Keck interferometer nuller (KIN) detected $10\ \mu\text{m}$ emission from two known disks – η Crv and γ Oph – and placed a $3\text{-}\sigma$ upper limit on the mean exozodi level at < 150 zodis (*Millan-Gabet et al.* 2011). Over the next few years, the Large Binocular Telescope Interferometer (LBTI) will conduct a similar survey with much better sensitivity, extending our knowledge of the exozodiacal luminosity function an order of magnitude lower (*Hinz et al.* 2008).

2.3. Near-Infrared Observations

Interior to the warm habitable-zone dust, a new category of systems with very hot dust (~ 1000 K) has been discovered via near-IR interferometry. The Vega system has been studied in the most detail, based on its detection with the CHARA interferometer (*Absil et al.* 2006). The best fit to its 1.3% excess at *K* band, combined with photometric upper limits at mid-IR wavelengths, is a disk with $\sim 1\ \mu\text{m}$ -sized grains piled up at an inner radius of 0.2 AU, roughly consistent with a sublimation temperature of 1700

K. Examples of other prominent debris disks with detected near-IR excess include τ Ceti (*di Folco et al.* 2007) and β Leo (*Akeson et al.* 2009). More broadly, *Absil et al.* (2013) have performed a near-IR survey of 42 nearby stars with CHARA, detecting excess for $28\pm 7\%$ of the targets. They find that near-IR excess is detected more frequently around A stars ($50\pm 13\%$) than FGK stars ($18\pm 7\%$). Interestingly, *K*-band excess is found more frequently around solar-type stars with detected far-IR excess, though not at a statistically significant level, and no such correlation is seen for A stars. Somewhat lower detection rates were obtained with a VLT/PIONIER survey in the *H*-band for a sample of 89 stars in the southern hemisphere, and the frequencies appear more uniform across the spectral types (*Ertel et al.* 2013). We discuss the origin of hot dust in § 7.

2.4. Impact of Stellar Metallicity and Multiplicity

In contrast to the well known positive correlation between giant planets and stellar metallicity, *Greaves et al.* (2006) and *Beichman et al.* (2006) found that the incidence of debris disks is uncorrelated with metallicity. These results are corroborated by subsequent works (*Maldonado et al.* 2012, and references therein). The only subtle difference might be a “deficit” of stars with disks at very low metallicities ($-0.50 < [\text{Fe}/\text{H}] < -0.20$) with respect to stars without detected disks (*Maldonado et al.* 2012), although this requires confirmation.

Debris disks are common around binary/multiple stars, giving information on the disks of multiple components that can be compared with those of protoplanetary disks (*Monin et al.* 2007). Statistically, *Trilling et al.* (2007) found an incidence rate of $\sim 50\%$ for binary systems (A3–F8) with small (< 3 AU) and large (> 50 AU) separations. They find a marginally higher rate of excess for old (age > 600 Myr) stars in binaries than for single old AFGK stars. In contrast, *Rodriguez and Zuckerman* (2012) found that *IRAS*-detected disks are less common around multiple stars (a result consistent with that of the DEBRIS survey, *Rodriguez et al.* 2013), and that, at any given age, the fractional luminosity of the dust in multiple systems is lower than in single stars, which would imply that disks around multiple systems are cleared out more efficiently.

A few multiple systems also host multiple disks, namely the δ Sculptoris quadruple system (*Phillips et al.* 2013) and the Fomalhaut tertiary system (*Kennedy et al.* 2013a).

2.5. Correlation with Exoplanet Populations

Many theories predict statistical relationships between planet and debris populations. Based on models of disk evolution as a function of disk mass/metallicity, *Wyatt et al.* (2007a) predict a correlation between planets and debris disk brightness. *Raymond et al.* (2012), on the other hand, predict that orbital instability among neighboring giant planets will produce an anti-correlation between eccentric Jupiters and debris disks, but a positive correlation between terrestrial planets and debris.

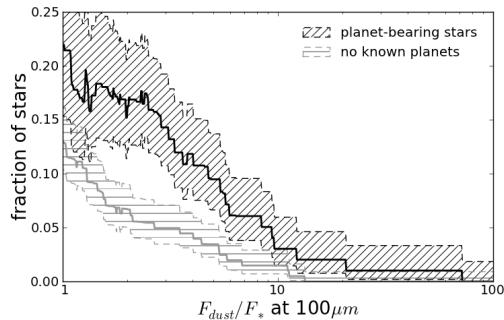


Fig. 4.— Stars that are known to have planets tend to have brighter debris disks. *Herschel* far-IR observations of planet-bearing stars (top curve) and stars not known to have planets (bottom curve) find that the disks’ fractional brightnesses ($F_{\text{dust}}/F_{\star}$ at $100\ \mu\text{m}$) are significantly larger for systems with planets (Figure credit: G. Bryden).

As a test of such theories, many attempts have been made to identify statistical correlations between debris and planet properties. While the long-period planets detected by direct imaging generally reside in prominent debris disks (e.g., β Pic and HR 8799; *Lagrange et al.* 2009; *Marois et al.* 2008), unbiased surveys with larger sample size are required to quantify any possible correlation. For this reason, debris disk surveys generally focus on planetary systems discovered via their induced radial velocities, such that the planets tend to orbit much closer to their central stars than outer debris detected in the far-IR. While initial *Spitzer* results found a relatively high detection rate of IR excess for known planet-bearing stars (*Beichman et al.* 2005b), analysis of the full set of *Spitzer* observations did not find a statistically significant correlation between planets and debris (*Bryden et al.* 2009; *Kóspál et al.* 2009). More recent analysis of *Spitzer* data combined with ongoing discoveries of lower mass planets, however, finds within the nearest 60 G stars a correlation between debris and the mass of a planet, where 4 out of 6 stars with only sub-Saturn-mass planets also have *Spitzer*-detected IR excess (*Wyatt et al.* 2012).

Within the *Herschel* key program surveys of nearby stars, 12 of 37 known planet-bearing stars are identified as having IR excess (*Marshall et al.* 2013). While this detection rate is not significantly higher than for other solar-type stars (20% within DUNES; *Eiroa et al.* 2013), debris disks are again found to be more common around systems with low-mass planets (*Moro-Martín et al.* 2013). Furthermore, combining the unbiased legacy surveys with *Herschel* observations of an additional 69 solar-type stars known to have planets reveals a statistically significant ($>3\text{-}\sigma$) correlation between the presence of planets and the brightness of orbiting debris (Fig. 4; *Bryden et al.* 2013). A planet-debris trend is also seen among *Herschel*-observed M stars, albeit with extremely small number statistics; in contrast to the 1% detection rate of IR excess for M stars not known to have planets (*Matthews et al.* 2013b), 1 of the 3 observed planet-

bearing M stars has detected debris (*Lestrade et al.* 2012).

3. DUST ORIGIN IN COLLISIONAL CASCADES

The baseline theoretical model for debris disks is that planet formation processes leave one or more belts of planetesimals orbiting the star, similar to the asteroid and Kuiper belts in the Solar System, that collide at sufficiently high velocities for those bodies to be destroyed, replenishing the dust that is observed. The process of grinding of larger bodies, planetesimals, into ever-smaller bodies, down to dust, is called a *collisional cascade*. This section presents analytic laws and reviews numerical modeling of such collisional cascades, showing how the complex interaction between different small body forces, and the composition and internal structure of those bodies, affect the structure and evolution of the disks and their observable properties.

3.1. Modelling Methods

Many properties of collisional cascades can be obtained analytically. However, the derivation of dust distributions with an accuracy sufficient to interpret the observations often necessitates numerical modeling of the cascade, together with radiation pressure and drag forces. Suitable numerical methods can be classified into three major groups.

N-body codes (e.g., *Lecavelier des Etangs et al.* 1996b; *Wyatt* 2006; *Krivov et al.* 2009; *Stark and Kuchner* 2009; *Thébaud* 2009; *Kuchner and Stark* 2010; *Thébaud* 2012; *Thébaud et al.* 2012) follow trajectories of individual disk objects by numerically integrating their equations of motion and store their instantaneous positions and velocities. Assuming that the objects are produced and lost at constant rates, this yields steady-state density maps of different-sized particles in the disk. Then, collisional velocities and rates can be computed and collisions can be applied to modify the collisionless distributions. This collisional “post-processing” can also be done iteratively. As the *N-body* methods are able to handle an arbitrary large array of forces, they are superior to the others in studies of structures in debris disks arising from interactions with planets, ambient gas, or interstellar medium, hereafter ISM (§6). However, they cannot treat a large number of objects sufficiently to cover a broad range of particle masses and often use rough prescriptions of collisional outcomes. As a result, an accurate characterization of the size distribution with *N-body* codes is not possible.

Statistical methods effectively replace particles with their distribution in an appropriate phase space. In applications to planetesimal and debris disks, one introduces a mesh of several variables comprising, for instance, mass, distance, and velocity (e.g., *Kenyon and Bromley* 2008, 2010; *Thébaud et al.* 2003; *Thébaud and Augereau* 2007; *Thébaud and Wu* 2008) or mass and orbital elements (*Krivov et al.* 2005, 2006, 2008; *Löhne et al.* 2012). The number of particles in each bin of the mesh at successive time instants is computed by solving equations that describe gain and loss of objects by collisions and other physical

processes. Statistical codes are much more accurate in handling collisions than N -body ones, but treat dynamics in a simplified way, for instance, by averaging over angular orbital elements. For this reason, they are less suitable for simulation of structures in debris disks.

In recent years, *hybrid codes* have been developed that combine accurate treatments of both dynamics and collisions (Kral *et al.* 2013; Nesvold *et al.* 2013). The basic construct in these codes is the superparticle (SP) (Grigorieva *et al.* 2007). An SP represents a swarm of like-sized particles sharing the same orbit which can be obtained through N -body integrations to account for all perturbations. Collisions between SPs in intersecting orbits are modeled by generating a set of new SPs that represent the modified remnants and newly born collisional fragments. The algorithm is complemented by procedures of merging similar SPs and deleting redundant or unnecessary ones to keep the total number of SPs at a computationally affordable level.

3.2. Steady-State Collisional Cascade

To model collisional cascades with statistical methods, one usually considers how mass flows between bins associated with objects of a given mass. Collisions lead to redistribution of mass amongst the bins. An important “reference case” is the steady-state collisional cascade, in which all bins gain mass from the break-up of larger bodies at the same rate at which it is lost in collisional destruction or erosion. Under the assumption that the fragment redistribution function (i.e., the size distribution of fragments from each collision) is scale-independent, the mass loss (or production) rate of a steady-state collisional cascade is the same in all logarithmic bins (Wyatt *et al.* 2011), with well characterized implications for the size distribution. In the absence of major collisional break-up events, a steady-state cascade represents a reasonable approximation to reality for all sizes with collisional timescales that are shorter than the age over which the cascade has been evolving.

3.3. Size Distribution

A steady-state cascade gives a size distribution of solids that is usually approximated by a power law, $n(D) \propto D^{-\alpha}$, or by a combination of such power laws with different indices in different size ranges. The index α does not usually have a strong dependence on the redistribution function, but is sensitive to the critical energy for fragmentation and dispersal, Q_D^* . If Q_D^* is independent of size, and neglecting the cratering collisions, then $\alpha = 3.5$ regardless of the redistribution function Dohnanyi (1969), as long as it is scale-independent. For $Q_D^* \propto D^b$, this generalizes to $\alpha = (7 + b/3)/(2 + b/3)$ (Durda and Dermott 1997; O’Brien and Greenberg 2003; Wyatt *et al.* 2011). With the typical values, $b \sim -0.3$ for objects in the strength regime ($D \lesssim 0.1$ km) and $b \sim 1.5$ for objects in the gravity regime ($D \gtrsim 0.1$ km), this leads to α between 3 and 4. Including further effects, such as the size-dependent velocity evolution of objects in the cascade, can somewhat flatten or

steepen the slope α , but usually does not drive α outside that range (e.g., Belyaev and Rafikov 2011; Pan and Schlichting 2012). For $3 < \alpha < 4$, the cross section, and thus the amount of observed thermal emission or scattered light, are dominated by small grains, while most of the mass resides in the biggest solids.

For dust sizes below 1 mm non-gravitational forces modify the size distribution. Radiation pressure effectively reduces the mass of the central star by a factor $1 - \beta$, where $\beta = 1.15 Q_{\text{pr}}(D)(L_*/L_\odot)(M_\odot/M_*)(1 \text{ g cm}^{-3}/\rho)(1 \mu\text{m}/D)$, with Q_{pr} being the radiation pressure efficiency averaged over the stellar spectrum, and ρ standing for grains’ bulk density. As a result, dust released from parent bodies in nearly circular orbits immediately acquire eccentricities $e = \beta/(1 - \beta)$. Thus if $\beta \geq 0.5$, the grains will be blown away on hyperbolic orbits. The corresponding size D_{bl} , referred to as the blow-out size ($\sim 1 \mu\text{m}$ for Sun-like stars), is a natural lowest cutoff to the size distribution, since the amount of grains with $D < D_{\text{bl}}$ is by several orders of magnitude (the ratio of the collisional lifetime of bound grains to the disk-crossing time of unbound ones) smaller than that of the bound grains. Note that for solar-type stars, very small grains ($D \ll D_{\text{bl}}$) may also stay in bound orbits, as their β becomes smaller than 0.5 at least for some material compositions. Furthermore, for later-type stars $\beta < 0.5$ at all sizes; the fate of submicrometre-sized motes in disks of these stars is unknown.

Thus a reasonable approximation to the size distribution is to use $\alpha = 3.5$ (or the appropriate slopes in the strength and gravity regimes) from the largest planetesimals involved in the cascade (i.e., those whose collisional lifetime is shorter than the time elapsed after the ignition of the cascade) down to the blow-out size (see e.g., the simulations for $\tau > 10^{-6}$ and $e = 0.1$ of Fig. 5a). This can particularly be helpful in estimating the total disk mass from the dust mass that can be inferred from submillimeter observations (e.g., Wyatt and Dent 2002; Krivov *et al.* 2008). However, the non-gravitational forces acting on μm -sized grains further modify the size distribution at these sizes.

A natural consequence of mass loss rate being independent of size in logarithmic bins when a cut-off below some minimum particle size is imposed is that the size distribution becomes wavy (Campo Bagatin *et al.* 1994; Wyatt *et al.* 2011). The shape of the size distribution close to the blow-out limit would be complicated by a natural spread in mechanical strength, optical properties, and even the densities of individual dust grains in realistic disks. The waviness also depends on the treatment of cratering collisions, since it does not arise in the simulations of Müller *et al.* (2010), and see also Figure 5a.

Whether the waviness exists or not, caution is required when using a single power-law down to D_{bl} . The blowout limit is not sharp, and the maximum in the size distribution can be shifted to larger sizes, both in disks of low dynamical excitation (§4.2), and in transport-dominated disks (e.g., Krivov *et al.* 2000), either because of the disks’ low optical depth or because transport mechanisms are partic-

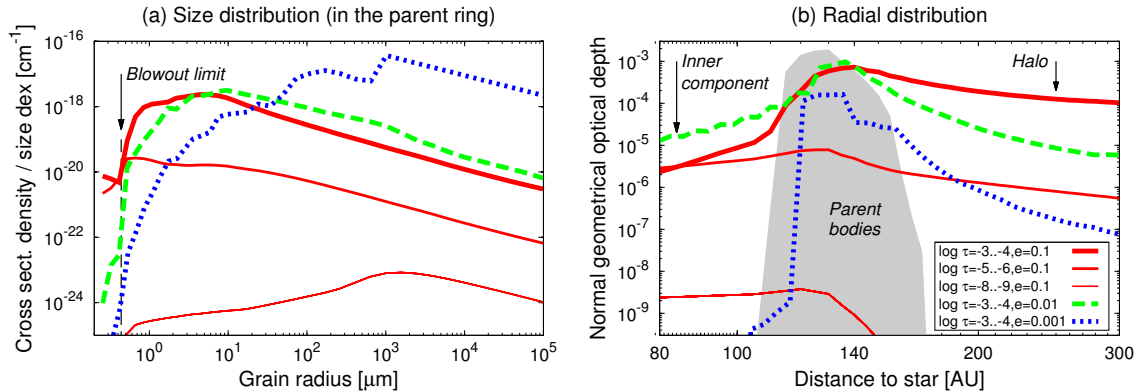


Fig. 5.— Typical size distribution (left) and radial profile (right) for fiducial disks with a 130 AU radius around a Sun-like star. All disks were generated numerically with a collisional code ACE (Krivov *et al.* 2005, 2006, 2008; Müller *et al.* 2010; Löhne *et al.* 2012) and evolved until a quasi-steady state at dust sizes were reached. Dust (and planetesimals) were assumed to be a mixture of astrosilicate and water ice in equal mass fractions. Disks have different peak optical depths (thick lines: $\tau \sim 10^{-3} \dots 10^{-4}$, medium lines: $\tau \sim 10^{-5} \dots 10^{-6}$, thin lines: $\tau \sim 10^{-8} \dots 10^{-9}$), and dynamical excitations (solid: $e \sim 2I \sim 0.1$, dashed: 0.01, dotted: 0.001). The figure demonstrates that both in weakly-stirred and transport-dominated disks the dominant grains sizes get larger (left), and the outer halos weaker (right). (Figure credit: A.V. Krivov)

ularly strong (e.g., owing to strong stellar winds that amplify the Poynting-Robertson (P-R) effect, Plavchan *et al.* 2005). Figure 5a shows that this effect is evident both for the $\tau < 10^{-8}$ and $e = 0.001$ simulations.

Even in a transport-dominated disk, the largest planetesimals are dominated by collisions. This is because the lifetime against catastrophic collisions in a disk with a size distribution slope $\alpha < 4$ increases more slowly with particle size, $T_{\text{coll}} \propto D^{\alpha-3}$ (e.g., Wyatt *et al.* 1999), than the transport timescale, $T_{\text{drag}} \propto D$. Defining the size D_c to be that at which the two timescales are equal (i.e., $T_{\text{coll}} = T_{\text{drag}}$), for a disk to have particles of any size in the transport dominated regime requires $D_c > D_{\text{bl}}$. The rough criterion for this (assuming transport to be caused by the P-R force) is $\tau < v/c$, where τ is normal geometrical optical depth, v is the circular Keplerian velocity at the disk radius, and c is the speed of light (Kuchner and Stark 2010). At sizes $D < D_c$, the slope $\alpha = \alpha_c - 1$, where α_c is the slope of the redistribution function (Wyatt *et al.* 2011), meaning that it is grains of size $\sim D_c$ that dominate the cross section.

3.4. Radial Distribution

Collisions, together with radiation pressure and drag forces, set not only the size distribution, but also the radial distribution of dust. As long as transport is negligible (i.e., $T_{\text{drag}} \gg T_{\text{coll}}$), a narrow parent belt of planetesimals should be surrounded by a halo of small grains in eccentric orbits, with pericenters residing within a “birth ring” and the apocenters located outside it (Lecavelier des Etangs *et al.* 1996a). The smaller the grains, the more extended their halo. Assuming $\alpha \approx 3.5$, the radial profile of dust surface density (or the normal optical depth) in such a halo should be close to $\tau \propto r^{-1.5}$ (Strubbe and Chiang 2006; Krivov *et al.* 2006); see e.g., the $\tau > 10^{-4}$, $e = 0.1$ simulation of Fig. 5b. For comparison, the halo formed by un-

bound grains on hyperbolic orbits would exhibit a flatter falloff, $\tau \propto r^{-1}$ (e.g., Lecavelier des Etangs *et al.* 1998).

In the opposite limiting case of a transport-dominated disk (i.e., $T_{\text{drag}} \ll T_{\text{coll}}$), drag forces steepen the profile of the halo to $\tau \propto r^{-2.5}$ (Strubbe and Chiang 2006; Krivov *et al.* 2006) and the inner gap of the birth ring (see the lower τ simulations of Fig. 5b) is filled by dust with a nearly uniform density profile, $\tau \propto r^0$ (e.g., Briggs 1962) — which can, of course, be altered by planets if any orbit in the gap (§6). Since a disk’s fractional luminosity is $f_d \approx (\tau/2)(dr/r)$, where dr is the characteristic disk width, many of the debris disks observed by *Herschel* at $f_d \sim 10^{-6}$ (see §2.1) have optical depths such that $T_{\text{coll}} \sim T_{\text{drag}}$. For such low density disks, one expects both a “leak” of dust inward from the parent ring location and a halo of small grains spreading outward.

The slopes, and the extent, of both the halo and inward leak components depend not only on $T_{\text{coll}}/T_{\text{drag}}$ (see Wyatt 2005b), but also on many other factors. Major — and essentially unknown — ones are again the level of stirring of dust-producing planetesimals (characterized by their typical eccentricities e and inclinations I) and their mechanical strength (i.e. Q_D^*). The stirring level and Q_D^* both determine the degree of “destructiveness” of the collisions and, through that, strongly affect both the size and radial distribution of dust. As an example, lowering the stirring level would largely suppress the outer halos.

3.5. Observational Constraints on Dust Properties

The models above describe the size and spatial distribution of dust. These already rely on a vast number of parameters and assumptions, most of which are poorly known or not known at all. These are mostly related to the largest planetesimals (e.g., their bulk composition, mechanical strength, primordial size distribution, dynamical

excitation, as well as location, width, and total mass of the belts), possible planetary perturbers that would affect the disks, and even the central stars (ages, stellar mass loss rates etc.). However, there is another important unknown, namely the properties of the observable dust (e.g., shape, porosity, chemical composition).

In the discussion above we tacitly assumed that the observations are sensitive to the cross-sectional area of the dust. This would be the case if the dust acts like a blackbody, but the situation is more complicated in ways that need to be understood if observations are to be correctly interpreted. For a start, the small particles that dominate the cross-section are inefficient emitters, which means that they emit at a temperature above blackbody (see also §5.1). This fact means that the SED, which constrains the disk temperature, can be used in concert with a disk radius measured directly from imaging to constrain the particle size distribution (e.g., *Wyatt and Dent* 2002, who found a size distribution slope $\alpha \approx 3.5$ for Fomalhaut) and composition (e.g., porous grains constituting a heterogeneous mixture of silicates, carbonaceous compounds, and ices have been favored for HD 181327 and HD 32297, *Lebreton et al.* 2012; *Donaldson et al.* 2013).

Additional information can be gained from scattered light and polarimetric data. *Hinkley et al.* (2009) use ground-based polarimetry to image the HR 4796A disk, measuring its scale height and determining that the disk is dominated by micron-sized grains, while *Maness et al.* (2009) find that sub-micron sized grains dominate the asymmetric disk of HD 61005. *Graham et al.* (2007) use polarized imaging with *HST* of the AU Mic disk to reveal that the disk is significantly ($> 300\times$) depleted of scattering material inside the 40 – 50 AU birth ring (*Strubbe and Chiang* 2006). The source of the emission is found to be highly porous (91-94%), micron-sized grains (with an upper size of decimeters for the parent bodies) in an optically thin disk. *Shen et al.* (2009) use random aggregates to model the AU Mic data and find these require a lower porosity of just 60% in 0.2 – 0.5 micron-sized grains.

The chemical composition of the debris dust can be directly probed by the presence of emission features in the spectrum. This composition should trace that of planetesimals, and thus its knowledge could give cosmochemical and mineralogical hints to the processes and conditions from the protoplanetary phase (*Dutrey et al.* 2014; *Pontoppidan et al.* 2014), including possible radial mixing and thermal history. The chemical composition of dust, together with – equally unknown – grain shape and porosity determines radiation pressure strength and D_{bl} , absorption efficiency in both the optical range and in the IR and so the dust temperature and thermal emission efficiency. It also affects the mechanical strength of the particles as, for instance, silicate particles show different collisional outcomes than icy grains (*Kilias et al.* 2013).

Direct probes of composition through solid state features are rare, however. Apart from the β Pic (*de Vries et al.* 2012) and possibly HD 181327 (*Chen et al.* 2008) disks,

this method is confined to systems with hot dust emitting in the mid-IR (see §7), for which the $10\mu\text{m}$ silicate feature is an important diagnostic of the dust composition and size. For instance, the presence of the silicate feature requires grains with radii $\lesssim 10/2\pi \mu\text{m}$, and so relatively few A stars with $10 \mu\text{m}$ excess exhibit strong silicate features (*Chen et al.* 2006; *Morales et al.* 2009). Less luminous stars, on the other hand, can more easily maintain small grains; later-type stars with $10\mu\text{m}$ excess generally have silicate features. Yet, in some systems the discovery of sharp features uncovers a problem that grains producing them must be smaller than the blowout limit (e.g., *Fujiwara et al.* 2012), contrary to the theoretical expectation that such grains should be underabundant.

The shapes of these features allow distinct mineral species to be identified and enables comparative astrogeology between systems and a consideration of their evolutionary state. *Spitzer* spectra of dust around HD 69830, for example, were originally explained by cometary parent bodies (*Beichman et al.* 2005a), but more detailed analysis subsequently found evidence of olivines, pyroxenes, and sulfides but no water ice, consistent with break-up of a C-type asteroid (*Lisse et al.* 2008; *Beichman et al.* 2011). The spectrum of HD 172555, on the other hand, is dominated by silica with a size distribution heavily weighted toward fine grains (*Lisse et al.* 2009). The impact velocities required to produce this composition also imply that the dust was created by a large (>150 km radius) asteroid impact. See *Lisse et al.* (2012) for a compilation of mid-IR spectra.

For disks without the benefit of direct imaging or spectroscopy, the degeneracy between particle size and disk radius, as well as the dust optical properties, means that none of these properties can be well constrained. Yet it is possible to estimate the sizes of emitting grains from the shape of the SEDs. Submillimeter data can be fit using a modified blackbody approximation, in which the flux longward of wavelength λ_0 is divided by a factor $(\lambda/\lambda_0)^{-\beta}$ where β is the emissivity power index. The measured β values are typically lower than the value of 2 observed for ISM grains (e.g., *Andrews and Williams* 2005), suggesting debris disk grains are larger than those populating the ISM. The λ_0 value can be thought of as representative of the grain sizes, and the values vary significantly. *Booth et al.* (2013) find $\lambda_0 \sim 70\text{--}170 \mu\text{m}$ and $\beta \sim 0.7\text{--}1.6$, as is consistent with many measured values for debris disks. In HR 8799, the best fit yields $\lambda_0 \sim 40 \mu\text{m}$, likely indicative of the small-grain dominated halo’s contribution to the SED’s cold component (*Matthews et al.* 2013a).

4. BIRTH AND EVOLUTION OF DEBRIS DISKS

4.1. Observations of the Transition Phase

At the young end, it is appropriate to pose the question: when is a disk a debris disk as opposed to a late-stage protoplanetary disk (or a “transition disk”, *Espaillet et al.* 2014)? Several studies have measured the disk frequency in young clusters and these convincingly show that 50% of proto-

planetary disks (as identified by a large near-IR excess from dust close to the star) are lost by 3 Myr, and that the fraction remaining is negligible by 10 Myr (Haisch et al. 2001; Hernández et al. 2007). Measurements of disk masses from submillimeter data (which probe the outer disk regions) also indicate that the 10 Myr age is significant (see Fig. 3, Panić et al. 2013). Indeed, the TW Hydra Association (~ 8 Myr, Zuckerman and Song 2004), hosts stars in the protoplanetary phase, such as TW Hydrae itself (Hughes et al. 2008b; Rosenfeld et al. 2012; Andrews et al. 2012) and in the debris phase, such as HR 4796A and TWA 7 (Schneider et al. 1999, 2005; Matthews et al. 2007; Thalmann et al. 2011) as could be expected within this transition period (Riviere-Marichalar et al. 2013).

4.2. Stirring

To produce dust by collisions, planetesimals in debris disks must have relative velocities sufficient for their fragmentation, i.e., the disks must be stirred. They may be *pre-stirred* by processes acting during the protoplanetary phase (Wyatt 2008). In typical protoplanetary disk models, relative velocities of solids are set by turbulence, Brownian motion, and differential settling and radial drift. This means that for mm-sized grains at ~ 100 AU, they are expected to lie in the m s^{-1} range (Brauer et al. 2008). This translates to eccentricities and inclinations $e \sim I \sim 0.001$. While there may be additional sources of velocity excitation that are not considered in such models, for example additional excitation from binary companions (Marzari et al. 2012; Thébault et al. 2010), the pre-stirring level is not expected to be much higher than $e \sim I \sim 0.01 - 0.001$ if planetesimals are to form by coagulation (e.g., Brauer et al. 2008; Zsom et al. 2010, 2011), unless collective dust phenomena are invoked (see Chiang and Youdin 2010, for a review).

The activation of disks some time after gas dispersal is usually referred to as *delayed stirring* (Dominik and Decin 2003). One viable mechanism could be *stellar flybys* (Kenyon and Bromley 2002). Since the timescale of cluster dissipation is $\lesssim 100$ Myr (Kroupa 1995, 1998), the ignition of the cascade by flybys can be expected to occur early in the systems' history. At that time, stars may experience encounters at various distances R , with several hundreds of AU probably being typical for a low- to medium-density cluster. Each encounter truncates the disk at $r \sim 0.3R$, and the zone between $\sim 0.2R$ and $\sim 0.3R$ becomes the most excited, and thus the brightest during that "encounter era". However, because the collisional depletion time at that region is also the shortest, that part of the disk is short-lived. What remains afterwards is a weakly excited disk inside $\sim 0.2R$, where the dynamical excitation scales as $e \propto r^{5/2}$ (Kobayashi and Ida 2001).

At later times, assuming a standard picture of collisional growth following planetesimal formation, it is expected that eventually the planetesimals will grow large enough to stir the debris disk, so-called *self-stirring* (Kenyon and Bromley 2010; Kennedy and Wyatt 2010). Formation of 1000 km-

sized planetesimals is normally considered sufficient to trigger the cascade. In the models of Kenyon and Bromley (2008), assuming a standard minimum-mass solar nebula with a solid surface density of $\sim 1M_{\oplus} \text{ AU}^{-2} r^{-3/2}$ around a solar-mass star, such objects would form on a timescale $\sim 400(r/80 \text{ AU})^3$ Myr. This suggests that Pluto-size objects can grow quickly enough to explain the dust production in Kuiper belt-sized disks starting from ages of 100s of Myr. These self-stirring models also predict an increase in disk radius with age, which has been suggested by some observations (see §4.4), although Wyatt et al. (2007b) noted that the rapid decay of close-in disks (see §4.4) means that the mean radius of detectable disks should increase with age, even if the disks themselves are not changing in radius.

Alternatively or in addition to self-stirring, *planetary stirring* by planets in the system is possible (Mustill and Wyatt 2009). The secular perturbations from a planet with mass m_{pl} , semimajor axis a_{pl} , and eccentricity e_{pl} stir the disk (see Fig. 7) on a timescale $\propto r^{9/2}/(m_{\text{pl}}e_{\text{pl}}a_{\text{pl}}^3)$ to $e \sim 2(a_{\text{pl}}/r)e_{\text{pl}}$. This timescale may be shorter than the self-stirring timescale for systems with a moderately eccentric planet orbiting close to the inner edge of the disk (like Fomalhaut) and even for systems with a close-in radial velocity planet in a more eccentric orbit (like ϵ Eri).

4.3. Disks at Different Stirring Levels

In the debris disk of our solar system, the EKB, both self-stirring and planetary stirring mechanisms are at work, and the stirring level is high. The resonant and scattered populations acquired their $e \sim I > 0.1$ from Neptune, while cold classical EKB objects have $e \sim I \lesssim 0.1$ consistent with self-stirring by their largest embedded members ($D \lesssim 200$ km). It is also possible that the Sun was born in a massive cluster and that flybys played a significant role in the early history of the EKB (e.g., Dukes and Krumholz 2012). In contrast, the origin of stirring in extrasolar debris disks remains completely unknown. Case studies (e.g., Müller et al. 2010; Wyatt et al. 2012) and interpretations of debris disk statistics (e.g., Wyatt et al. 2007c; Löhne et al. 2008; Kennedy and Wyatt 2010) have shown that both self-stirring and planet-stirring models are consistent with the available data. The true level of stirring is not known either. Most of the "pre-Herschel" models assumed values at the EKB level, $e \sim I \sim 0.1$. However, recent discoveries of disks with sharp outer and smooth inner edges, and those of thermally cold disks, have challenged this assumption. It is therefore important to review how the level (and origin) of stirring affect the disk observables.

If the dust-producing planetesimals have a low dynamical excitation which, however, is still high enough for collisions to be mostly destructive, then the low collision velocities between large grains, that are not susceptible to radiation pressure, would decrease the rate at which small grains are produced. However, the destruction rate of these small grains is set by eccentricities induced by radiation pressure and remains the same (Thébault and Wu 2008). This

should result in a dearth of small dust. The maximum of the size distribution shifts to larger values (Fig. 5a), and the outer edge of the disks, formed by small “halo” grains, gets sharper (Fig. 5b). This is the scenario favored in the collisional simulations of *Löhne et al.* (2012) who modeled the *Herschel* disk around a Sun-like star HD 207129 (*Marshall et al.* 2011). Their best match to the data assumed a dynamical excitation at the $e \sim I \sim 0.03$ level, for which the dominant grain size lies at $\approx 3\text{--}4 \mu\text{m}$.

At a stirring level below $e \sim I \sim 0.01$, i.e. at random velocities below a few tens m s^{-1} , collisions are not necessarily destructive — with the caveat that the collisional outcome, and thus the fragmentation threshold, depend on many factors which include not only the impact velocity, but also the impact angle, masses, materials, porosities, morphology, and hardnesses of projectile and target (*Blum and Wurm* 2008). At $e \sim I \sim 0.001$, i.e., at the level consistent with the natural pre-stirring from the protoplanetary phase, impact experiments in the laboratory reveal a rather complex mixture of outcomes, including disruption, cratering and bouncing with mass transfer, and agglomeration in comparable fractions (*Güttler et al.* 2010). Using these results, *Krivov et al.* (2013) considered belts of primordial grains that could have grown on the periphery of a protoplanetary disk (where stirring from close-in planets, if any, is negligible) to sizes larger than $\sim 1 \text{ mm}$ (to avoid the gas or radiative drag losses), but smaller than $\sim 1 \text{ km}$ (to keep self-stirring at a low level). Their collisional simulations demonstrate that such a belt can largely preserve the primordial size distribution over Gyrs, with only a moderate accretional growth of the largest solids and a moderate production of collisional fragments in the submillimeter range (Fig. 5b, dotted line). The existence of such belts was previously predicted by *Heng and Tremaine* (2010), who considered a regime in which collisions are low enough in velocity for the outcome of collisions to be bouncing rather than fragmentation (or accretion). This scenario may provide an explanation for *Herschel* observations that identified several candidate “cold disks” where the emitting dust material is nearly as cold as blackbody and thus should be dominated by large grains (*Eiroa et al.* 2011, 2013).

4.4. Evolution on the Main Sequence

The large samples of main-sequence stars observed for IR emission have built up a picture of how debris disks evolve over time. It has been conclusively shown that excess rates decrease with the age of the stars independently of spectral type (e.g., *Su et al.* 2006; *Wyatt et al.* 2007b; *Trilling et al.* 2008; *Carpenter et al.* 2009; *Chen et al.* 2011, 2012; *Urban et al.* 2012). The decline of the incidence rate, which was already noticed in *ISO* surveys (e.g., *Habing et al.* 2001), is significant up to ages $< 1 \text{ Gyr}$ but it is not apparent for older ages (*Trilling et al.* 2008). Such a non-obvious decay is also supported by the *Herschel* DUNES survey (*Eiroa et al.* 2013).

The decline in excess emission is observed to be much

faster at $24 \mu\text{m}$ than at $70 \mu\text{m}$ for A stars (*Su et al.* 2006). *Thureau et al.* (2013) also note an apparent decline in the excess at 100 and $160 \mu\text{m}$. The decay timescales increase with wavelength. The upper envelope to the ratio of observed flux to photospheric flux at each wavelengths can be approximated by decay curves of $1 + t_0/t$, where t_0 is 150, 400 and 800 Myr , for 24 , 70 and $100/160 \mu\text{m}$, respectively. Among A stars in the DEBRIS survey, the incidence rate for stars $< 450 \text{ Myr}$ is double that of stars $> 450 \text{ Myr}$, but substantial levels of excess are still observed for the oldest stars in the sample ($\sim 800 \text{ Myr}$). For FGK stars, *Carpenter et al.* (2009) and *Siegler et al.* (2007) both find that $24 \mu\text{m}$ excesses decline with age for the FEPS targets and a compilation of FGK stars observed with *Spitzer* respectively, whereas *Hillenbrand et al.* (2008) do not see such an apparent trend in the FEPS sun-like stellar sample at $70 \mu\text{m}$.

Many studies do not find any trend in disk properties such as temperature with the stellar temperature or age (e.g., *Hillenbrand et al.* 2008; *Trilling et al.* 2008; *Lawler et al.* 2009; *Chen et al.* 2011, 2012; *Dodson-Robinson et al.* 2011; *Moór et al.* 2011b), regardless of the nature of the dust (i.e., cold or warm). *Rhee et al.* (2007) and *Moór et al.* (2011b) claim however that for early and late-type stars, respectively, there is an increase of the radial location of the dust with the stellar age. In addition *Herschel* DUNES results suggest that there might exist trends between the mean blackbody radius for each F, G and K spectral types, and a correlation of disk sizes and an anticorrelation of disk temperatures with the age (*Eiroa et al.* 2013). At submillimeter wavelengths, *Nilsson et al.* (2010) find an evolution of disk radii with age (for $< 300 \text{ Myr}$ stars) in contrast with the results from *Najita and Williams* (2005).

The observed decay of debris disks with time is expected, because planetesimal families undergo collisional depletion over long time spans and are not replenished. Useful analytic scaling laws that describe timescales of the quasi-steady state evolution of collision-dominated disks have been worked out (*Wyatt et al.* 2007c; *Löhne et al.* 2008; *Krivov et al.* 2008). For example, for a narrow parent ring with initial mass M_0 and radius r , at a time t_{age} from the onset of the cascade,

$$F(xM_0, r, t_{\text{age}}) = xF(M_0, r, xt_{\text{age}}), \quad (1)$$

$$F(M_0, xr, t_{\text{age}}) = F(M_0, r, x^{-13/3}t_{\text{age}}), \quad (2)$$

where $x > 0$ is an arbitrary factor, and $F(M_0, r, t)$ stands for any quantity directly proportional to the amount of disk material, such as the total disk mass, the mass of dust and its total cross section. Equation (2) explains why the fastest declines occur in warm dust that is located closer to the star, while the colder outer dust remains to much later times.

One consequence of these scalings is that, once the largest planetesimals have come to collisional equilibrium, the dust fractional luminosity should decay as $f_d \propto t_{\text{age}}^{-1}$, and that there is a maximum possible fractional luminosity

at any t_{age} (Wyatt *et al.* 2007c):

$$f_{\text{max}} = 2.4 \times 10^{-8} \left(\frac{r}{\text{AU}} \right)^{7/3} \left(\frac{dr}{r} \right) \left(\frac{D_{\text{max}}}{60 \text{ km}} \right)^{0.5} \\ \times \left(\frac{Q_{\text{D}}^*}{300 \text{ J/kg}} \right)^{5/6} \left(\frac{e}{0.1} \right)^{-5/3} \left(\frac{t_{\text{age}}}{\text{Gyr}} \right)^{-1}, \quad (3)$$

for a central star with solar mass and luminosity. These results are valid under certain assumptions, including independence of Q_{D}^* on size, as well as the requirement that the collisional lifetime of the largest planetesimals $T_{\text{coll}}(D_{\text{max}})$ is shorter than t_{age} . More detailed models that lift these assumptions predict shallower decay laws, $f_{\text{d}} \propto t_{\text{age}}^{-0.3 \dots -0.8}$, and allow f_{max} to be, by about an order of magnitude, larger than equation (3) suggests (Löhne *et al.* 2008; Gáspár *et al.* 2013). Yet these results imply that the hot dust in some systems, having $f_{\text{d}} \gg f_{\text{max}}$, cannot stem from a steady-state cascade in “asteroid belts” close to the stars (see §7).

These models for the long term collisional evolution of planetesimal belts have been particularly useful for the interpretation of statistics on the incidence of debris as a function of age. They have been taken as the basis of population synthesis models (analogous to population synthesis models used to explain exoplanet populations, Benz *et al.* 2014) that can reproduce the observed evolution, and in so doing provide information on the distribution of planetesimal belt radii and largest planetesimal sizes (Wyatt *et al.* 2007b; Löhne *et al.* 2008; Kains *et al.* 2011; Gáspár *et al.* 2013).

4.5. Debris Disks around Post-Main Sequence Stars

Observational evidence of disk evolution after the main sequence phase has advanced significantly since PPV when there was one detected disk around a white dwarf (Zuckerman and Becklin 1987). Debris disks now have been detected around many white dwarfs (Dufour *et al.* 2012; Kilic *et al.* 2005, 2006; Kilic and Redfield 2007), including those at the centre of planetary nebulae (Su *et al.* 2007; Bílková *et al.* 2012), primarily in the near- and mid-IR. In fact, the growth in the body of work on this subject is such that it could encompass a chapter unto itself, and we can only scratch the surface here.

Typical incidence rates for warm debris disks around cool white dwarfs are on the order of 1% (Girven *et al.* 2011; Kilic *et al.* 2009). Barber *et al.* (2012) estimate a disk incidence rate of $4.3^{+2.7}_{-1.2}\%$ in a metallicity unbiased sample of 117 cool, hydrogen-atmosphere white dwarfs. Many detected disks have gaseous as well as solid components (Brinkworth *et al.* 2012). Gänsicke *et al.* (2008) find that the hydrogen-to-metal abundance in a white dwarf gas disk is more than 1000 times below Solar, supporting the idea that these disks of dust and gas are created by the disruption of rocky planetesimals.

In addition to dust in orbital configurations, an increasing number of studies demonstrate that tidally stripped asteroids or planetary material has been deposited on the surface of white dwarfs themselves (Zuckerman *et al.* 2003; Graham *et al.* 1990). This type of “pollution” provides

important compositional information about rocky bodies in planetary systems. Significant numbers of metal-contaminated white dwarfs are now known, and many of these are now known to have IR excesses, detected from ground-based facilities or *Spitzer*. Based on *K*-band data, Kilic and Redfield (2007) suggest the incidence rate of debris disks around DAZ (hydrogen-dominated atmosphere) white dwarfs is $\sim 14\%$.

Several authors have modeled the evolution of such disks. The debris present should be a descendent of the main sequence debris population, but the physics is not yet fully understood; Bonsor and Wyatt (2010) looked at the evolution of the population of planetesimals known around main sequence A stars and their detectability due to collisions and the changing radiation and wind forces throughout the post main sequence, while Dong *et al.* (2010) modeled the dynamical evolution of a debris/giant planet system through to the white dwarf phase, predicting final debris ring sizes of 30-50 AU. Models for the transport of material onto the star explain transport rates consistent with what can be provided through PR drag (Rafikov 2011a), but a number of stars are observed to have higher accretion rates that are not so readily explained (Rafikov 2011b). Metzger *et al.* (2012) suggest that sublimation of solids enhances the gas component of the disk, leading to runaway accretion; coupled with a long metal settling phase on the star, this could explain the polluted white dwarfs that do not show IR excess.

5. RESOLVED DISKS AND DISK STRUCTURE

In 2005, the year of the PPV meeting, the submillimeter camera SCUBA (Holland *et al.* 1998) was retired from JCMT. SCUBA had been the most effective imaging instrument for debris disks, resolving more than half of the 14 systems imaged at that time. Excepting β Pic and Fomalhaut, each disk was resolved at a single wavelength only. Nearly a decade later, significant strides have been made in resolving disk structures, owing to ongoing campaigns on *HST* (e.g., Hines *et al.* 2007; Maness *et al.* 2009) and ground-based instruments in the optical (e.g., Buenzli *et al.* 2010, VLT), near-IR (e.g., Janson *et al.* 2013; Thalmann *et al.* 2011), mid-IR (e.g., Smith *et al.* 2009; Moerchen *et al.* 2010; Smith *et al.* 2012) and (sub)millimeter (e.g., Maness *et al.* 2008; Wilner *et al.* 2012; MacGregor *et al.* 2013). *Spitzer* also contributed to the resolved images library, resolving several disks, many with multiple components (Vega, HR 8799, Fomalhaut, Su *et al.* 2005, 2009; Stapelfeldt *et al.* 2004, respectively). Most notably, the launch of *Herschel* in 2009 has yielded a vast gallery of resolved disks; both the DUNES and DEBRIS key programs have resolved a half of the detected disks (i.e., Matthews *et al.* 2010; Eiroa *et al.* 2010; Marshall *et al.* 2011; Eiroa *et al.* 2011; Churcher *et al.* 2011; Wyatt *et al.* 2012; Löhne *et al.* 2012; Lestrade *et al.* 2012; Kennedy *et al.* 2012a,b; Eiroa *et al.* 2013; Broekhoven-Fiene *et al.* 2013; Booth *et al.* 2013). *Herschel* has also produced the first resolved debris

disk around a sub-giant, κ CrB (*Bonsor et al. 2013a*) and a resolved image of the gas-rich debris disk 49 Ceti (*Roberge et al. 2013*).

Such emphasis is placed on resolved disk images because of the immense amount of information that can be gleaned from them compared to an SED alone. Resolving disks even marginally at one wavelength places very meaningful constraints on the disk structure, for example giving a direct measure of the radial location of the dust, but resolving disks at multiple wavelengths at high resolution allows significant observational constraints on the radial and temperature structure of disks, as well as their component grain sizes and compositions. Azimuthal variations, warps and offsets between the disk and star can also be evidence of unseen planets in such systems (see §5.5 and §6).

5.1. The Physical Extent of Disks

Measured sizes of debris disks from resolved images are consistently larger than those inferred from SED analyses in which temperature (typically found in the range $\sim 40 - 200$ K) is used as a proxy for radial separation from the star and the dust grains are assumed to be blackbodies. Grains are typically greybodies, meaning they exhibit a warmer temperature than a blackbody given their distance from the parent star (see § 3.5). It is therefore not surprising that the ratio, Γ , of the radius measured from the image to that inferred from the disk temperature assuming blackbody grains, is often greater than unity. *Booth et al. (2013)* show Γ to range from 1–2.5 for nine resolved A stars in the DEBRIS survey. *Rodriguez and Zuckerman (2012)* find ratios as high as 5 in their sample of IRAS binary star disk-hosts. These results are consistent with typical grain size being on the order of microns, roughly comparable with the radiation pressure blowout limit discussed in §3.

The resolved physical extent of disk emission typically ranges from 10s to 1000s of AU from the parent star, but it is important to differentiate this emission from the underlying distribution of planetesimals, which is best traced by longer wavelength observations of larger (and typically cooler) grains, as we discuss below.

5.2. Planetesimal Rings, Belts and Gaps

Many disks show evidence for a narrow birth ring, harbouring planetesimals on nearly circular orbits, as the underlying sources of the debris disk material (e.g., *Strubbe and Chiang 2006*). Collisional modeling for the disks of Vega (*Müller et al. 2010*) and HD 207129 (*Löhne et al. 2012*) demonstrates that these are compatible with a steady-state collisional cascade in a narrow planetesimal annulus, even though the dust distribution appears broader. An appreciable spread of the dust sheet should be naturally caused by radiation pressure and drag forces acting on collisional fragments, and may be either outward (Vega) or inward (HD 207129) from the birth ring, as discussed in §3, and see Figure 5b.

In systems without detected planets, one of the key mea-

surable quantities is the sharpness of the inner edge, which sets constraints on the mass of any planet if it sits close to the inner edge of the belt (*Chiang et al. 2009*), as discussed further in §6. Figure 6 shows one of the first resolved images from ALMA, which promises to be a key instrument in the resolution of planetesimal belt locations around nearby stars. The combination of long observing wavelengths and high resolution places significant constraint on the belt width (13-19 AU) and reveals the sharpness of both the inner and outer boundary (*Boley et al. 2012*). In addition, ALMA imaging of the AU Mic debris disk has firmly placed the planetesimal belt at 40 AU for that edge-on system, and a second, unresolved component centred on the star could be a warm, asteroid belt (*MacGregor et al. 2013*).

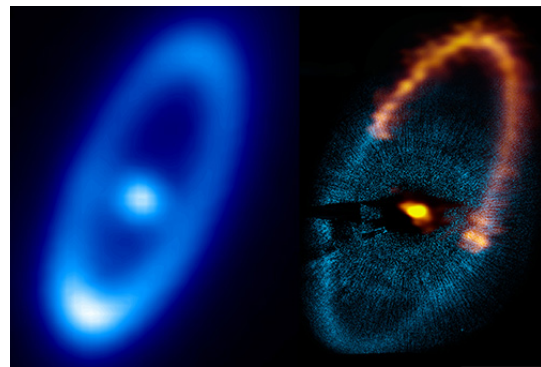


Fig. 6.— The (left) *Herschel* 70 μm (*Acke et al. 2012*) and (right) composite *HST*/ALMA 850 μm (*Kalas et al. 2005*; *Boley et al. 2012*) images of Fomalhaut reveal the impact of observing wavelength and resolution on the detected structure. Both *Herschel* and ALMA have sufficient sensitivity to detect an unresolved central component (associated with the warm dust seen at 24 μm by *Stapelfeldt et al. 2004*) and show sharp inner edges and the offset of the ring from the central star first detected by *HST*. It is this offset and the obvious brightness asymmetry of the disk seen by *Herschel* which strongly support the case for an unseen planet in the Fomalhaut system. (Figure credits: *Herschel*, ESA/Herschel/PACS/B.Acke/KU Leuven; ALMA, ESO/NOAJ/NRAO; *HST*, NASA/ESA)

For many of the disks resolved by *Herschel*, however, the cold dust emission is not consistent with distribution in a narrow ring — even when taking into account that the distribution of dust is usually broader than that of the parent planetesimals. The full sample of resolved disks around A stars between 20–40 pc (from the DEBRIS sample) reveal that only three of the nine systems are well fit by narrow rings, while four definitely require multiple rings to explain the observations (*Booth et al. 2013*).

Such systems can instead be explained as a broad belt. Such a disk can be modeled with a set of non-interacting narrow radial annuli, and the same models of §3 can be applied, allowing one to predict the radial distribution of dust (e.g., *Kennedy and Wyatt 2010*; *Wyatt et al. 2012*).

Sufficiently close to the star, where $T_{\text{coll}}(D_{\text{max}}) < t_{\text{age}}$, eq. (3) suggests that the radial profile of the dust optical depth should be rising outward as $\tau \propto r^{7/3}$. Farther out – at the distances which have already been reached by the stirring front (§4.2), but the largest planetesimals have not yet started to deplete collisionally – a profile that is flat or declining with radius is expected for $\tau(r)$. This shows a possible way of explaining inner gaps in debris disks by collisional erosion, i.e., without the assistance of planets (see §6).

However, within the limits of low resolution imaging, broad disks could alternatively be interpreted as multiple belts, and there is evidence for this in the SEDs of some disks (e.g., *Hillenbrand et al.* 2008). *Morales et al.* (2011) studied a sample of B8-K0 stars, many of which contain both warm and cold dust, reminiscent of the two-belt debris architecture of the Solar System. Fitting the SEDs of these two-belt systems, *Morales et al.* (2011) find a bimodal distribution to the measured dust temperatures (their Fig. 2), where ~ 50 K cold belts are distinct from ~ 200 K warm belts, although *Ballering et al.* (2013) find less distinction in temperature. The break between the two populations occurs at the same temperature for both solar-type and A-type stars, whereas the dust location varies considerably with spectral type if other grain properties, e.g., optical constants or size distribution, are ignored. *Morales et al.* (2011) suggest that the break in temperatures is related to the ice line at ~ 150 K, either by setting the location for dust-releasing comet sublimation or by creating a favorable location for giant planets to form and remove neighboring debris.

Evidence for multiple, narrow components in well resolved images of disks are becoming abundant and provide more definitive evidence of the presence of gaps or holes from which dust is excluded (i.e., *Moro-Martín et al.* 2010). For example, in addition to cold dust components, both Vega and Fomalhaut exhibit warm (170 K) dust, identified with *Spitzer* (*Su et al.* 2013; *Stapelfeldt et al.* 2004), and hot dust, revealed by $2 \mu\text{m}$ excess (see §2.3; *Absil et al.* 2006; *di Folco et al.* 2004). *Su et al.* (2013) show that the three components are spatially separated with orbital ratios of ~ 10 . Even richer, and more reminiscent of the Solar system, is the architecture of the HR 8799 system, with warm and cold disk components (*Su et al.* 2009; *Reidemeister et al.* 2009; *Matthews et al.* 2013a) and four planets between them (*Marois et al.* 2008, 2010).

5.3. Halos

Halos refer to disk components detected at very large distances from a star, typically far beyond the expected location of a planetesimal belt. The origin of halos is readily explained by the collisional processes that create grains close to the blow-out size. These grains are pushed outward by radiation pressure to extended elliptic or even hyperbolic orbits, to distances far outside the birth ring (see §3). The first image of a debris disk around β Pic was due to its extended halo seen in scattered light (*Smith and Ter-*

rile 1984), which typically extends further in radius than thermal emission. Halos have now also been detected in emission, however (e.g., Vega, *Sibthorpe et al.* 2010). The resolved disk thermal emission toward HR 8799 was identified with *Spitzer* to extend to 1000 AU (*Su et al.* 2009); *Herschel* data resolve a very extended halo with an outer bound of 2000 AU (*Matthews et al.* 2013a), more extensive than the scattered light halo around β Pic. Interestingly, the halo is not distinct from the planetesimal belt in temperature, and HR 8799’s SED is well fit by two temperature components, one of warm dust close to the star (*Su et al.* 2009) and the other a cold outer component. Radial profiles reveal the distinction in the distribution around 300 AU between the shallower profile of the planetesimal belt and the steep profile of the halo (*Matthews et al.* 2013a).

Not all disks have extended halos. The absence of a detectable halo can equally be attributed to a low stirring level of dust-producing planetesimals (e.g., *Löhne et al.* 2012), to grains that are mechanically “harder” than assumed, to the dearth of high- β grains caused by their peculiar composition, or even to strong stellar winds that might enhance the inward drift of grains by the P-R effect in some systems (e.g., *Augereau and Beust* 2006; *Reidemeister et al.* 2011).

5.4. Disk Orientation

One of the fundamental unknowns is the inclination of the disk system relative to us, which can be estimated straightforwardly from a well-resolved image with an underlying assumption of a circular disk. There is growing evidence that most systems in which inclinations have been measured for disks and stars independently show no evidence of misalignment (*Watson et al.* 2011; *Greaves et al.* 2013). There are also examples of systems in which the star, planets and disk are all aligned (*Kennedy et al.* 2013b). Thus for systems with radial velocity planets, resolving a disk in the system provides an inclination which (if shared) can better constrain the masses of the planets, which are lower limits when it is unknown. However, misaligned disks are occasionally detected. For example, *Kennedy et al.* (2012a) present a steady-state circumbinary polar-ring model for the disk around 99 Herculis based on *Herschel* observations, in contrast to the coplanar systems around two other DEBRIS resolved disks in binary systems (*Kennedy et al.* 2012b).

5.5. Asymmetric Structures

Resolved imaging can highlight areas of dust concentration and avoidance. These locations frequently exhibit strong asymmetries in emission, such as eccentric offsets, inclined warps, and dense clumps. It is worth noting that the presence of planets in both the β Pic (*Heap et al.* 2000) and Fomalhaut (*Kalas et al.* 2005; *Quillen* 2006) systems was predicted based on asymmetries in their disk structures, and companions were subsequently found in both disks (*Lagrange et al.* 2010; *Kalas et al.* 2008).

The best known case for an eccentric ring is Fomalhaut

(see Fig. 6), but other systems have now been observed to show such offsets, i.e., HR 4796A (Thalmann et al. 2011), HD 202628 (Krist et al. 2012) and ζ^2 Ret (Eiroa et al. 2010). The classic example of a warped disk is β Pic (Heap et al. 2000), which was later revealed to have two distinct disk components, one inclined to the main disk (Golimowski et al. 2006) but aligned with the orbit of the detected planet (Lagrange et al. 2012).

In the nearby disk around ϵ Eridani, significant clumpy structure has been observed at multiple wavelengths, most strikingly in the submillimeter (Greaves et al. 1998). Due to the close proximity of this star (3.3 pc), its high proper motion allows the confirmation that some of the clumps are co-moving with the star (Greaves et al. 2005). It is also possible to search for evidence of orbital rotation of these features, which is currently detected at 2-3 σ significance both for ϵ Eridani (Poulton et al. 2006) and for a clump in the β Pic disk (Li et al. 2012).

Generally, the most easily observed asymmetry is a difference in brightness of one side of the disk over another. As discussed in §6, particles on eccentric orbits have an asymmetric distribution around the star and glow near the pericenter due to their higher temperature there. Very little eccentricity need be imposed on the dust to create this effect (e.g., β Leo, Churcher et al. 2011). Giant planets in young disks may even induce spiral structures, e.g., HD 141569 (Clampin et al. 2003).

Not all asymmetries need arise from planetary influence (see §6.4). Several resolved disks have been inferred to show structure resulting from interaction with the ISM, i.e., HD 15115 (Kalas et al. 2007; Rodigas et al. 2012), HD 32297 (Debes et al. 2009), and HD 61005 (Maness et al. 2009). Such ISM interactions do not preclude the presence of an underlying debris disk however; Buenzli et al. (2010) discovered an off-centre ring in the HD 61005 system with high-resolution imaging with the VLT, which could point to an underlying planetary companion.

6. PLANETARY AND STELLAR PERTURBATIONS

Most particles in a debris disk simply orbit the star on Keplerian orbits until the point at which they collide with another particle, at which point there is some redistribution of mass into particles that then follow new Keplerian orbits (see §3), usually only slightly modified from the original orbit unless the particles are small enough for radiation pressure to be significant. The dominant perturbation to this scenario in the Solar System comes from the gravitational perturbations of the planets. If a star has any planets in orbit around it, it is inevitable that its debris disk will be affected by such perturbations, since the debris orbits in a gravitational potential that is modified by the planets. Such perturbations can be split into three different components, both mathematically and physically (Murray and Dermott 1999), and each of these can be linked to specific types of structure that would be imposed on any gravitationally perturbed disk.

6.1. Secular Perturbations

These are the long-term effect of a planet's gravity, and are equivalent to the perturbations that would arise from spreading the mass of the planet along a wire that follows its orbit. For moderately circular and co-planar orbits, the effect of a planet's eccentricity and inclination are decoupled, but both play a similar role. Planetary eccentricities impose an eccentricity and pericentre orientation on all disk material, while planetary inclinations affect the orbital plane of that material. In the case of a single planet system, the disk tends to align with the planet. The alignment takes place on long timescales that also depend on distance from the planet. This means that the effect of a planet can cause disk evolution over 10s of Myr before it reaches steady state.

If a planet is introduced into a system on an orbital plane that is misaligned with the disk midplane, a warp will propagate through the disk (see Fig. 7), with more distant material yet to notice the planet and so retaining the original plane, and closer material already having been aligned with the planet. A warp at 80 AU was used to infer the presence of an inner planet in the 12 Myr-old β Pic disk at ~ 9 AU and 9 M_{Jup} (Mouillet et al. 1997; Augereau et al. 2001) that was later identified in direct imaging (Lagrange et al. 2010). Such a warp can also be a steady state feature in a system of multiple (misaligned) planets, though such a scenario also needs to acknowledge that the planets secularly perturb each other providing additional constraints (e.g., Dawson et al. 2012).

A planet that is introduced on an eccentric orbit causes a tightly wound spiral to propagate through a disk of planetesimals that were initially on circular orbits (see Fig. 7, Wyatt 2005a). The spiral is caused by differential precession between neighbouring planetesimal orbits, which eventually also causes these orbits to cross, potentially resulting in catastrophic collisions which can ignite a collisional cascade (see §4.2; Mustill and Wyatt 2009). In other words, secular perturbations allow a planet's gravitational reach to extend far beyond its own orbit.

On long timescales an eccentric planet will cause a disk to become eccentric. This may be observed as an offset centre of symmetry, or as the consequent brightness asymmetry caused by one side being closer to the star (Wyatt et al. 1999). Although such eccentricities were initially discussed from low significance brightness asymmetries in HR4796 (Telesco et al. 2000), the predicted offset in this system has now been confirmed (Thalmann et al. 2011), and the offset is quite striking in some disks (Kalas et al. 2005; Krist et al. 2012), and becoming more ubiquitous as disks can be imaged at higher resolution (see §5.5).

Secular perturbations from binary companions would play a similar role to that of a planet, though in this case the companion may be expected to have a relatively high eccentricity or inclination, resulting in the evolution of the eccentricities and inclinations of disk material being coupled. At high enough mutual inclinations, the character of the evolution changes dramatically as disk material under-

goes Kozai oscillations in which high inclinations can be converted into high eccentricities (Kozai 1962). It is notable that such large oscillations do not necessarily imply long-term instability, though this might not be compatible with a disk that is narrow both radially and vertically. However, there are solutions for circumbinary orbits for which narrow disks are possible. For example, there is a stationary (i.e., non-evolving) orbit that is orthogonal to the binary orbital plane, leading to the possibility that stable circumpolar rings may exist (Kennedy *et al.* 2012b, see §5.4).

The above discussion on structures from secular perturbations only considered the distribution of planetesimal orbits. In general the orbits of dust grains trace that of the planetesimals. However, the effect of radiation pressure does need to be taken into consideration, particularly where it is evident that observed structure originates from a halo component (see §5.3 and Nesvold *et al.* 2013).

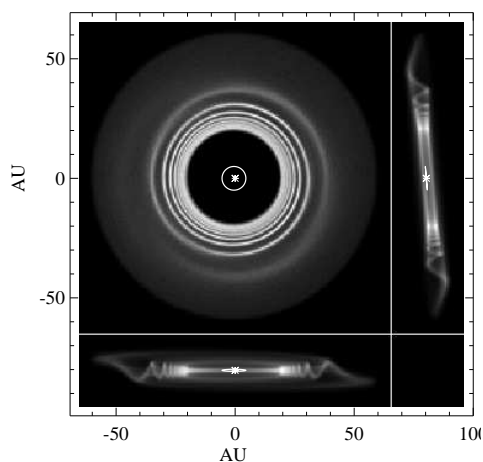


Fig. 7.— Structure of an initially coplanar low eccentricity 20 – 60 AU debris disk 100 Myr after the introduction of a 1 Jupiter mass planet on an orbit (shown in white) at 5 AU with eccentricity $e = 0.1$ and inclined 5° to the disk midplane. The planetesimals exhibit a tightly wound spiral structure far from the planet (Wyatt 2005), which is wound so tightly at the inner edge that the planetesimals are on crossing orbits ensuring destructive collisions (Mustill & Wyatt 2009). Coincident with the spiral is a warp (Augereau *et al.* 2001) with an appearance that depends on the viewer’s orientation to the line-of-nodes (see bottom and right panels for two different edge-on views). (Figure credit: M. Wyatt).

6.2. Resonant Perturbations

These arise at locations where debris orbits the star an integer (p) number of times for every integer ($p + q$) number of planet orbits. As this definition suggests there are an infinite number of resonances, but the strongest are usually the first order resonances (i.e., $q = 1$). As the example of the Plutinos in the EKB and the Kirkwood gaps

in the asteroid belt tell us, specific resonances can be either over- or under-populated. One location where resonances are always under-populated is close to a planet where, because resonances have finite width, the first order resonances overlap (Wisdom 1980). This overlap region is chaotic so debris does not remain there for long. The shape of this chaotic region has been the subject of much discussion, since the slope of the edge of the debris, and its offset from the planet, can be used to determine the mass of the planet – e.g., sharper edges require lower mass planets (Quillen 2006; Chiang *et al.* 2009), although there are degeneracies with the eccentricities of the planetesimals’ orbits (Mustill and Wyatt 2012).

It is generally suspected that planets shape the inner edge of debris disks, but it has yet to be demonstrated, and a debris disk that was born with a sharp inner edge would likely maintain it for several Gyr. Similarly, the fact that the debris in the Solar System traces the only regions of the Solar System that are stable over its 4.5 Gyr age (Lecar *et al.* 2001), is suggestive that extrasolar debris also traces regions of dynamical stability, and so that there are planets hiding in the gaps in the debris (Faber and Quillen 2007), causing instabilities due to both overlapping mean motion resonances and secular resonances (Moro-Martín *et al.* 2010). This is not necessarily the case, however, since debris may be absent from regions in between planets for reasons associated with the formation of the system.

A more specific observable caused by resonances is a clumpy structure. This is because of the special geometry of resonant orbits which have closed patterns in the frame rotating with the planet, with each resonance having its own geometry (i.e., its own clumpy pattern). Resonances occupy relatively narrow regions of parameter space, and to form a detectable clumpy structure these would have to be filled by resonance sweeping. For example, if a planet migrates through a disk, its resonances will sweep through the disk; some planetesimals can be trapped into resonance and migrate out with the planet (Malhotra 1993; Wyatt 2003). Because trapping probabilities into different resonances depend on the planet’s mass and migration rate (Wyatt 2003), as well as the particle eccentricity (Reche *et al.* 2008; Mustill and Wyatt 2011), these parameters can be constrained from observations of a clumpy structure; the planet’s location can also be pinpointed, since it will lie at a radial distance just inside the clumps, at an azimuthal angle that is evident from the clumpy structure, but generally lies far from clumps. An understanding of dust physics is also important for this comparison, since radiation pressure eventually causes the dust to fall out of resonance, so that observations at short enough wavelengths to probe small bound grains have an axisymmetric structure (Wyatt 2006; Krivov *et al.* 2007), while those that probe small unbound grains have spiral structure emanating from the clumps (Wyatt 2006). This can explain why disk structure is so wavelength dependent, and underscores the need for multi-wavelength imaging to constrain the models.

Another mechanism for resonance sweeping is dust mi-

gration through a disk by P-R drag; the dust crosses the resonances and becomes trapped thus halting the migration (Weidenschilling and Jackson 1993). Various papers have studied the structures expected in this case (Ozernoy et al. 2000; Quillen and Thorndike 2002; Kuchner and Holman 2003; Deller and Maddison 2005). Early papers ignored the importance of collisions, however, which tend to destroy particles in mutual collisions before they migrate far from their source in disks that are dense enough to detect (Wyatt 2005b). Fully consistent N-body simulations of this process that incorporate collisions are now being performed (Stark and Kuchner 2009; Kuchner and Stark 2010), confirming that this is an important factor, and concluding that clumpy structures formed by this mechanism kick in at densities below around 10^{-5} (see also Krivov et al. 2007).

There is controversy over some claims of clumps (Hughes et al. 2012), so it is important that the models make testable predictions. One of these is that the clumps should orbit the star with the planet.

6.3. Scattering

Scattering processes are those that are best visualized as the hyperbolic encounter of a planetesimal with a planet. This results in a large impulsive change in the planetesimal's orbit, and a minor change in that of the planet. In the Solar System, scattering is the dominant process governing the evolution of comets that are passed in from the EKB by interactions with the giant planets (Levison and Duncan 1997), which may also be true in extrasolar systems (see §7 and Davies et al. 2014). Another Solar System population dominated by scattering is the scattered disk of the EKB that extends out towards the Oort cloud through interactions with Neptune (Morbidelli et al. 2004). Planet formation may result in all systems having a scattered disk at some level, and indeed there is evidence in some planet formation models for mini-Oort clouds (Raymond and Armitage 2013). The collisional evolution of such high eccentricity populations has its own challenges, as discussed in Wyatt et al. (2010).

Scattering is also inevitable if a planet is placed in the middle of a debris disk, and can be invoked to place constraints on the presence of embedded planets. For example, a disk would be naturally broadened by such scattering, so a narrow disk requires the most massive object to be between Pluto and Earth. The recent discovery that Fomalhaut b crosses, and may even go through, its debris disk (Kalas et al. 2013) emphasizes that scattering processes may be a significant evolutionary mechanism.

If the debris disk is sufficiently massive, then multiple scatterings can significantly alter the orbit of an embedded planet. Typically the planet's eccentricity would be damped by dynamical friction and its semimajor axis would evolve, causing the planet to migrate (Fernandez and Ip 1984; Levison et al. 2007). The direction of the migration depends on various factors (Kirsh et al. 2009; Capobianco et al. 2011), and it is possible for a planet to migrate all the way to the

edge of a sufficiently massive debris disk (Gomes et al. 2004). The resulting migration could be invoked to cause resonance trapping (§6.2), though it is challenging to model this process due to the large number of planetesimals required to make the migration smooth enough for resonance trapping to occur.

The planet need not migrate far for this process to have a significant effect on the debris disk. For example, if there are multiple planets in the system, then this migration can push them towards an unstable configuration (Moore and Quillen 2013). In the Nice model for the Solar System, the ensuing instability resulted in the depletion of most of the mass of the EKB (Gomes et al. 2005). With the right configuration this instability could have been delayed for several 100 Myr, explaining the Late Heavy Bombardment (LHB). If such long delays are common in other systems there could be a signature of this in statistics, though this appears not to be the case because the primary consequence would be a sharp drop in the number of disks detected (Booth et al. 2009).

Scattering can also have a consequence on the distribution of dust, even if it no longer has an effect on the planetesimal belt; e.g., Thébaud et al. (2010) considered how the action of a planet exterior to a planetesimal belt would truncate the halo of small dust created in collisions in the belt and put onto high eccentricity orbits by radiation pressure (see also Lagrange et al. 2012).

6.4. Non-Gravitational Perturbations

It is worth pointing out that although the above discussion describes ways in which planets will inevitably impose structure on a debris disk, the existence of such features in a disk is not necessarily a signpost for planets, as there may be a non-planetary explanation. For example, clumps in debris disks can also arise from recent collisions (Wyatt and Dent 2002), though these are usually expected to be hard to detect except in the inner few AU (Kenyon and Bromley 2005). Confirmation of more systems in which structures can be linked to planets that are known from other means, such as the case of β Pic b, is needed for greater confidence in a planetary interpretation.

Non-gravitational perturbations can often be ruled out, but there are some that have already been shown to dominate the structure of some disks, most notably interaction with the ISM (Artymowicz and Clampin 1997). Bow shock-like structure can be evidence of interstellar dust streaming past the star that is deflected by radiation pressure (Gáspár et al. 2008). Forcing from the ISM can also have a secular effect on particle orbits (Maness et al. 2009; Debes et al. 2009) and is most important for low density disks (Marzari and Thébaud 2011). Of key importance to such analyses is the direction and speed of motion through the ISM, which is known for most nearby stars.

7. ORIGIN OF HOT DUST

The origin of hot dust around nearby stars remains a mystery, partly because its rarity and proximity to the star make it difficult to study. Regardless, its very existence causes some theoretical conundrums, and several models have been proposed to circumvent these.

7.1. Asteroid Belt

While it is tempting to interpret hot exozodiacal dust found at a few AU (§2.2) as asteroid belt analogues, such belts would rapidly deplete due to mutual collisions and so become undetectable within a few 10s of Myr (see eq. 3), and so it is not possible to explain hot dust around stars that are older than a few 100 Myr in this way (Wyatt *et al.* 2007c; Heng and Tremaine 2010). This is, however, a perfectly reasonable explanation for the hot dust found around young stars. The age up to which asteroid belt emission can be detected is a strong function of the radial location of the belt, but otherwise the main constraint is that sufficient mass remains in the belt at the end of planet formation. The ubiquity or absence of such belts could thus indicate whether planetary systems are commonly fully packed (leaving no regions of long-term dynamical stability in which an asteroid belt could reside) or are otherwise depleted by processes such as planet migration or secular resonance sweeping.

7.2. Terrestrial Planet Formation

Terrestrial planet formation (Raymond *et al.* 2014) is another model that can be invoked to explain the existence of hot dust around young stars, since the process of building up terrestrial planets by the coalescence of planetary embryos is thought to take 10 – 100 Myr. Many models of this process include a significant planetesimal population that co-exists with the embryos throughout this time, with a consequently high level of mid-IR emission from dust produced in collisions amongst this planetesimal population (e.g., Kenyon and Bromley 2004). Even if such planetesimals are not retained from the protoplanetary disk phase, collisions between the embryos are thought to have occurred as late as 50 Myr in the Solar System, the date of the Moon-forming collision. The debris produced in that collision would not be dynamically removed for 10s of Myr, and so unless the escaping debris is all placed in small objects that can then collisionally deplete very rapidly, this debris would be detectable for ~ 15 Myr (Jackson and Wyatt 2012). This is an exciting possibility, since it means that we can witness the aftermath of such massive collisions, and this has been proposed as the explanation of some hot excesses on compositional grounds (Lisse *et al.* 2008, 2009). However, this can also cause problems for planet formation models, because hot dust is found around just $\sim 1\%$ of young Sun-like stars (Kennedy and Wyatt 2013). This could mean that late giant collisions are rare, and that terrestrial planet formation is largely complete by the time the protoplanetary disk disperses (though see Rhee *et al.* 2008; Melis *et al.* 2010).

7.3. Cometary Populations

The fraction of dust in the Solar System’s zodiacal cloud that comes from asteroids and from comets is a matter for debate, but it seems that both contribute (Nesvorný *et al.* 2010). The main obstacle to resolving that question is how to model the production of cometary dust. In the context of extrasolar systems a bigger obstacle is the lack of knowledge about the planetary system, since that determines the rate at which cometary material is scattered into the inner system where it may be seen as a hot dust excess. However, this also introduces the exciting possibility that hot cometary dust, and how it relates to an outer Kuiper belt, can be used as a probe of the intervening planetary dynamics. Some progress has been made on understanding these dynamics recently, by using analytical considerations to assess how far in planetary systems can scatter comets, which depends on their spacing (Bonsor and Wyatt 2012), and N-body simulations to show that tightly packed systems of low mass planets would create high levels of hot dust (Bonsor *et al.* 2012). Nevertheless, further work is still needed on this process, including how to model the level of dust production by comets, which arises not just from sublimation, but also from disintegration, and (if the comet population is sufficiently massive) collisions.

7.4. Extreme Eccentricity Populations

A variant of the cometary explanation is the possibility that the comets are not continually being replenished from an outer belt, rather that they were implanted on highly eccentric orbits at the end of planet formation and have remained there ever since. Wyatt *et al.* (2010) showed that a population that has pericentres at ~ 1 AU, and apocentres at 100s of AU, could survive for Gyr of collisional evolution, with properties similar to those observed. The viability of this explanation thus rests on the likelihood that planet formation processes result in such a highly eccentric population. Such extreme eccentricities were not found in models that invoked planet migration (Payne *et al.* 2009), but planet-planet scattering may be a plausible formation mechanism (Raymond and Armitage 2013).

7.5. Dynamical Instability

The remaining explanations for hot dust around old stars envisage this as a transient population. One explanation is that there was a large influx of comets in a single event, possibly related to a dynamical instability in the planetary system, similar to the Late Heavy Bombardment experienced by the Solar System ~ 600 Myr after formation. Both modelling of the Solar System (Booth *et al.* 2009) and of instabilities in a larger set of planet formation models (Bonsor *et al.* 2013b), find that the resulting hot dust enhancement is relatively short-lived. Thus even if late stage instabilities were common (which we know they are not, Booth *et al.* 2009), there would be very few nearby stars currently undergoing this phenomenon. However, that does not exclude rare systems, such as η Corvi which has hot dust within

a massive Kuiper belt (Wyatt *et al.* 2005), being in such a state.

7.6. Recent Collisions

While collisions would have depleted an asteroid belt to below detectable levels, the proximity of the asteroid belt to the star means that it only takes the break-up of one relatively small asteroid (e.g., 10 – 100 km) to create an observable amount of dust (if it is broken into small enough fragments; e.g., *Kenyon and Bromley* 2005). Indeed, the evolution of the dust content of the asteroid belt is known to have been punctuated by many such events, visible today in the large body population as the Hiryama asteroid families (*Nesvorný et al.* 2003), and in the dust population as the dust bands (*Low et al.* 1984). Thus it is tempting to explain hot dust in this way (*Weinberger et al.* 2011), especially in systems like BD+20 307 and HD 69830 toward which we see no cold reservoir of planetesimals, as would be required by most other scenarios (though such a reservoir can have evaded detection, *Wyatt et al.* 2007c).

7.7. Temporal Evolution

One way to distinguish between the models will be to consider how the disks evolve with time (e.g., *Meng et al.* 2012). For example, as asteroid belts deplete, the frequency of the massive collisions considered in §7.6 also goes down. This means that for every 1–3 Gyr collision there would be 10 times more in the 0.3 – 1 Gyr age range. The age dependence of this phenomenon is not well characterized due to small number statistics, but the existence of several > 1 Gyr hot dust systems argues against such a dramatic decline. However, this age dependence does not hold if the parent bodies are large enough, and few enough, to be stranded from collisional equilibrium constraints (e.g., *Kennedy and Wyatt* 2011). Thus an origin in collisions between planetary embryos, rather than between the largest members of an asteroid belt, remains a plausible explanation, if planet formation models can be shown to retain such embryos for Gyr.

The discovery of a hot disk undergoing rapid decay is a significant advance that remains without adequate theoretical explanation (*Melis et al.* 2012). If such rapid evolution is the norm, this would require revision to the models that attempt to explain hot dust. *Kennedy and Wyatt* (2013) also pointed out that another way to characterize the way hot disks evolve is to look at the frequency of fainter disks; those that are detectable with current technology are the outliers, but if they are transient they must evolve through lower levels of excess that can be detectable.

7.8. Extremely Hot Dust

The majority of the discussion above focussed on dust that is at ~ 1 AU. However a more ubiquitous phenomenon seems to be the excess inferred to be an order of magnitude closer to the star (see §2.3; *Absil et al.* 2013). The explanations for this excess would be broadly similar to those outlined above, with typically more stringent constraints.

However, in this case it might be possible to invoke processes related to the star itself, rather than a debris disk (e.g., *Cranmer et al.* 2013).

8. GAS IN YOUNG DEBRIS DISKS

8.1. Observations

The gas-to-dust ratio of most debris disks is not well constrained. While the disks are identified based on their dust emission, there are relatively few detections of accompanying gas. Indeed, debris disks are sometimes defined as being gas-poor. The best example of a gas-bearing debris disk is the young β Pic system (~ 12 Myr; *Zuckerman et al.* 2001), where small amounts of gas have been identified via UV/optical absorption lines for a range of species (e.g., CaII, NaI, CII, CIII, and OI; *Hobbs et al.* 1985; *Roberge et al.* 2006). The velocity structure of the disk has recently been mapped in CO with ALMA (*Dent et al.* 2013). Absorption by molecular hydrogen, however, is not detected (*Lecavelier des Etangs et al.* 2001). While observations of absorption lines can provide a very sensitive tracer of orbiting gas (indeed, β Pic’s gas was detected before its IR excess; *Slettebak* 1975), they require alignment of the disk with the line-of-sight; emission line measurements are more effective at ruling out gas for systems not viewed edge-on. These longer wavelength emission measurements, however, are limited to specific temperatures/regions of the disk. Mid-IR spectra, for example, are generally sensitive to warm (100s of K) gas, while millimeter observations probe colder material. For this reason, *Pascucci et al.* (2006) used a comprehensive approach – combining *Spitzer* spectra (H_2 at $17 \mu\text{m}$, [Fe II] at $26 \mu\text{m}$, and [SI] at $25.23 \mu\text{m}$) with millimeter observations of ^{12}CO transitions – to place gas limits on a sample of young stars. For their ~ 10 -100 Myr disks, they rule out gas masses more than a few M_{\oplus} for the outer disk (10 – 40 AU) and constrain the surface density at 1 AU to be $< 1 \text{ g/cm}^2$, i.e. $< 10^{-4}$ of the MMSN.

While most debris disk observations are consistent with the early removal of most gas (at ages $\lesssim 10$ Myr), 49 Ceti appears to be an exceptional case. One of only two debris disks with detected CO emission (also HD 21997; *Moór et al.* 2011a), 49 Ceti is the oldest known disk with significant amounts of gas (~ 40 Myr; *Zuckerman and Song* 2012). Its resolved CO emission is modelled as a gas disk extending out to 200 AU, with an empty region within 40 AU (*Hughes et al.* 2008a). The presence of a significant amount of gas at such an age has implications for the formation of giant planets. If the gas is primordial, i.e., there is a large amount of hydrogen alongside the CO, then the total gas mass is estimated at $\sim 10 M_{\oplus}$ (*Hughes et al.* 2008a). While this is not enough to form a Jupiter-mass planet, it could easily supply the envelope for Neptune/Uranus analogs ($\sim 1 M_{\oplus}$ of hydrogen). On the other hand, *Herschel* recently made the first detection of ionized carbon emission from the disk, at $158 \mu\text{m}$ (*Roberge et al.* 2013). The [OI] $63 \mu\text{m}$ line, however, was unexpectedly not detected, suggesting an enhanced C/O ratio. Thermal modeling of the

overall dataset (lines plus the resolved dust emission) suggests that the source of the gas may be cometary, rather than primordial (Roberge et al. 2013).

8.2. Origin of Gas

It cannot be completely ruled out that what is observed is unusually long-lived remnants of the protoplanetary disks. Indeed the fact that the gas and dust in HD 21997 are not co-spatial argues for a primordial origin for some of its gas (Kóspál et al. 2013). Also, about ten Earth masses of gas, if not more, could still remain in many young debris disks where gas was searched for and not found, without violating observations (Hillenbrand 2008). However, there are more arguments in favor of secondary, rather than primordial, origin of the observed gas (Fernández et al. 2006). For instance, CO observed around β Pic (Vidal-Madjar et al. 1994; Jolly et al. 1998; Roberge et al. 2000), 49 Cet (Hughes et al. 2008a) and HD 21997 (Moór et al. 2011a), should be photodissociated on timescales of hundreds of years in the absence of shielding (van Dishoeck and Black 1988; Roberge et al. 2000; Moór et al. 2011a) and thus likely needs continuous replenishment.

Evaporation of short-period and especially infalling comets, as inferred from observed variable absorption lines of β Pic (e.g., Ferlet et al. 1987; Beust and Valiron 2007), can certainly contribute to the observed gas, but – as long as the process only works close to the star – is unable to explain why gas is observed so far from the star, as inferred from the double-peaked line profiles of β Pic (Olofsson et al. 2001) and HD 21997 (Moór et al. 2011a).

To account for similarity between the gas and dust distributions, Czechowski and Mann (2007) proposed vaporization of solids in dust-dust collisions. However, the typical threshold speed for vaporization by pressurizing shocks is a few km/s for ice and in excess of 10 km/s for silicate and carbon (Tielens et al. 1994). Thus this mechanism can only work very close to the stars where the Keplerian speeds are high – or in exceptionally dusty disks, such as β Pic’s, where abundant high-speed β -meteoroids (grains put on hyperbolic trajectories by radiation pressure, see §3) are predicted to sweep through the disk and vaporize bound grains.

One more possibility is photon-stimulated desorption of dust, which can release various species such as sodium, observed around β Pic (Chen et al. 2007). This process requires strong UV emission from the star, which would be consistent with the fact that gas has been detected predominantly in debris disks of A-type stars.

Collisions of volatile-rich dust grains can also release gas through sublimation, rather than collisional vaporization. In contrast to protoplanetary disks, the gas pressure in debris disks is very low. As a result, sublimation occurs at lower temperatures. For instance, ice sublimates at ~ 100 – 110 K instead of 145 – 170 K as in protoplanetary disks (Lecar et al. 2006). The sublimation distance for “dirty” (organics-coated) ice bodies ranges from 20 – 35 AU for $L_* < 30L_\odot$ and $65(L_*/100L_\odot)^{1/2}$ AU for

$L_* \gtrsim 30L_\odot$ (Kobayashi et al. 2008). The sublimation distances are similar for ammonia ice, and is even larger for other ices such as CO (Dodson-Robinson et al. 2009). CO ice, in particular, sublimates at temperatures as low as 18 – 35 K and thus would vaporize in EKB-sized debris disks even around solar-type stars following collisions between the dust grains. However, the gas production rate needed to account for the amount of CO observed around 49 Cet (Hughes et al. 2008a) and HD 21997 (Moór et al. 2011a), is by at least an order of magnitude larger than the estimated dust production rate. To mitigate the problem of a relatively rapid rate of CO production (compared to dust production rate), Zuckerman and Song (2012) suggested that most of CO is produced in collisions of larger, cometary bodies that sequester CO in their deeper, sub-surface layers. Indeed, the mass loss rate is the same in all logarithmic bins of a steady-state collisional cascade (see §3.2; Wyatt et al. 2011). Assuming that the gas production rate is a fixed fraction of the mass loss rate, the gas production rate in collisions of all bodies from, say, $1 \mu\text{m}$ to 10 km in size can easily be by an order of magnitude larger than in collisions of dust grains in the $1 \mu\text{m}$ – $10 \mu\text{m}$ range.

All the processes outlined above should occur in every disk at some level. The only question is how efficient they are and how that efficiency depends on the system’s parameters (e.g., system age, stellar luminosity, disk radius, disk mass). For example, the mechanisms differ in whether they result from interaction of a single solid object (a dust grain or a comet) with the radiation field or require pairwise collisions between such solids. These two types of processes would imply that the gas production efficiency scales with the amount of solids linearly and quadratically, respectively. Unfortunately, with only a few “gaseous” debris disks discovered so far, the statistics are too scarce to identify the dominant process based on this argument. Nor is it clear whether the same or different mechanisms are responsible for the gas production in these systems. Finally, it is debated whether gas production at observable levels occurs in a steady state regime or if it is only observed in those systems where a major “stochastic” event recently occurred, such as an individual collision between two gas-rich comets or even planetary embryos (Moór et al. 2011a; Zuckerman and Song 2012).

8.3. Dynamical Effect on Dust

Assuming gas is not influenced by dust, dust “aerodynamics” was laid down by Weidenschilling (1977) mostly for protoplanetary disks. This treatment was generalized to optically thin disks, where dust is subject to radiation pressure, by Takeuchi and Artymowicz (2001). They pointed out that, while the motion of gas is sub-Keplerian (usually due to the pressure gradient), that of dust grains is sub-Keplerian, too, because of the radiation pressure. Sufficiently small grains should be slower than the gas. As a result, while larger grains drift inward, grains smaller than several times the blowout size should spread outward. Us-

ing these results, *Thébaud and Augereau* (2005) described the radial profile of dust distribution in a debris disk with gas, attempting to put an upper limit on the gas density from the observed scattered-light brightness profiles in resolved disks. *Krivov et al.* (2009) revisited the issue by considering a wide range of gas densities, temperatures, and compositions. They showed that, although individual trajectories of grains are sensitive to these parameters, the overall dust distribution remains nearly the same. They concluded that the observed brightness profiles of debris disks do not pose stringent constraints on the gas component in the systems.

Once the gas-to-dust ratio becomes comparable to unity, it is vital to include the back reaction of gas from dust. Gas drag is known to concentrate dust at pressure maxima (*Takeuchi and Artymowicz* 2001). If the disk is optically thin to the stellar light, and the star emits enough in UV, gas is mainly heated by dust through photoelectric heating. In this case, the larger the dust concentration, the hotter the gas, and the higher the pressure, which causes the dust to concentrate more, creating an instability (*Klahr and Lin* 2005; *Besla and Wu* 2007; *Lyra and Kuchner* 2013). This has been suggested as a “planetless” explanation for rings and spirals seen in systems like HR 4796A, HD 141569, and β Pic.

The key problem with all the models of gas-dust interaction is that, for a standard primordial composition, most of the gas mass should be contained in hydrogen. Its amount is hard to measure directly, and it is difficult to deduce it from the observed species, since H_2/CO and other ratios in debris disks are not reliably known.

9. SUMMARY/OUTLOOK

The past decade has brought a wealth of new data and modeling advancement for the study of debris disks as components of extrasolar planetary systems. Much of this has been achieved with data from the space-based IR surveys of *Spitzer*, *Herschel* and *WISE*, windows which are now closed for the foreseeable future. While *Meyer et al.* (2007) tabulated 14 resolved debris disks around other stars, disks have now been resolved around nearly 100 nearby stars, many at multiple wavelengths. These resolved images effectively break the degeneracies inherent in modeling the disks for dust location and grain sizes. Many resolved cold disks are being found to have inner, warm disk components as well. The HR 8799 system, with warm and cold debris components with 4 gas giant planets between them is very similar to the solar System, but exhibits an extended halo seen around several, predominantly A type, stars.

Ground-based facilities are now coming to the fore, however, which promise even better sensitivity and the resolution of disk structures which are key to any in-depth study of individual disks and the detection of signatures associated with planets. Advances made possible by interferometers over a large range of wavelengths (i.e., LBTI, VLTI, CHARA, and ALMA and JVLA) will be particularly illuminating. At short wavelengths, interferometers probe the

presence of hot dust, and its origins are clearly a key question to be addressed in the coming decade. At long wavelengths, ALMA will provide unprecedented resolution of cold disk components, including potentially the position of the central star through detection of warm inner components in the same observation (*Boley et al.* 2012; *MacGregor et al.* 2013). High resolution imaging of disks will also be possible through facilities such as JWST, CCAT and GPI (Gemini Planet Imager).

There are several key questions that are likely to be the focus of study in the coming decade. One of the most challenging will be: what is the main mechanism that stirs debris disks: planets, embedded big planetesimals or both? And what range of stirring levels is present in disks? The challenge for theoretical models will be to balance detailed studies of the dynamical and collisional evolution of specific systems, with the need to explain observations of the broad ensemble of disks in such a way that meaningful constraints can be extracted on the underlying physics. For example, disks are seen to become fainter, and potentially larger, with age, as expected for material undergoing collisional evolution in a steady state. However, as the disks are being characterized in ever increasing detail, it is clear that we do not yet have an explanation for the diverse properties of their halos, and an explanation for the range of disk widths and the relation between multiple components (and the implications of such components on our interpretation of the statistics) are still to be found.

Cold and hot disk components appear to be detected toward 20-30% of stars, with rates higher toward A stars, while warm dust components are detected $\sim 10\times$ less frequently. Measured incidence rates are suggestively lower around solar-type stars, but not statistically so, and current surveys have failed to detect significant numbers of disks around M stars, most exceptions being very young, although they lack the sensitivity to fractional luminosities around M stars comparable to earlier spectral types. Thus, the true incidences of cold and warm debris dust remain not entirely clear, and the potential differences of disk frequencies among stars of different spectral types are still awaiting explanation.

Recent work suggests a positive correlation between debris disks and planets where the most massive planet in the system is a Saturn mass or less (*Wyatt et al.* 2012; *Moro-Martín et al.* 2013), and *Herschel* data show a statistically significant correlation between planets and the brightness of debris (*Bryden et al.* 2013), as predicted by *Wyatt et al.* (2007c). However, whether or not the presence of dusty debris around a star implies the existence of planets remains an open question.

A related, more focussed issue for modelers and observers is whether inner cavities or gaps in debris disks are indeed populated by planets. Direct imaging of planets will not be possible for all systems, but higher resolution disk images can solidify the link between disk structures and underlying planet populations. Eccentricities of disks can place significant constraints on the mass and orbits of inner

planets, as can the sharpness of the inner disk edges when resolved. In addition, the warps and offsets which were the fingerprints of planets in the β Pic and Fomalhaut systems can be discerned in other systems when higher resolution images are available.

A traditional hallmark of debris disks has been the absence of detected gas in most systems. *Herschel* and now ALMA have made significant progress toward the detection of various species in the debris disks β Pic and 49 Ceti, both previously known gas hosts. Both are relatively young, which may be a pre-requisite for detected gas in debris systems.

In addition to the disks detected around white dwarfs, metal-rich white dwarfs themselves may be a class related to the debris disk phenomenon. Such stars may be “polluted” by the deposition of material from planetesimals onto the stellar surface. These objects therefore provide another means of probing the composition of planetesimals in extrasolar debris disk systems.

Acknowledgments CE is partly supported by the Spanish grant AYA 2011-26202. AVK acknowledges support from DFG grant Kr 2164/10-1. MCW is grateful for support from the EU through ERC grant number 279973.

REFERENCES

- Absil O. et al. (2006) *AAp*, 452, 237.
 Absil O. et al. (2013) *AAp*, 555, A104.
 Acke B. et al. (2012) *AAp*, 540, A125.
 Akeson R. L. et al. (2009) *ApJ*, 691, 1896.
 Andrews S. M. and Williams J. P. (2005) *ApJ*, 631, 1134.
 Andrews S. M. et al. (2012) *ApJ*, 744, 162.
 Anglada-Escudé G. and Tuomi M. (2012) *AAp*, 548, A58.
 Artymowicz P. and Clampin M. (1997) *ApJ*, 490, 863.
 Augereau J. and Beust H. (2006) *AAp*, 455, 987.
 Augereau J.-C. et al. (2001) *AAp*, 370, 447.
 Aumann H. H. (1985) *PASP*, 97, 885.
 Avenhaus H. et al. (2012) *AAp*, 548, A105.
 Ballering N. P. et al. (2013) *ApJ*, 775, 55.
 Barber S. D. et al. (2012) *ApJ*, 760, 26.
 Beichman C. A. et al. (2005a) *ApJ*, 626, 1061.
 Beichman C. A. et al. (2005b) *ApJ*, 622, 1160.
 Beichman C. A. et al. (2006) *ApJ*, 652, 1674.
 Beichman C. A. et al. (2011) *ApJ*, 743, 85.
 Belyaev M. A. and Rafikov R. R. (2011) *Icarus*, 214, 179.
 Benz W. et al. (2014) *Protostars and Planets VI*, in press.
 Besla G. and Wu Y. (2007) *ApJ*, 655, 528.
 Beust H. and Valiron P. (2007) *AAp*, 466, 201.
 Bilíková J. et al. (2012) *ApJS*, 200, 3.
 Blum J. and Wurm G. (2008) *ARAA*, 46, 21.
 Boley A. C. et al. (2012) *ApJL*, 750, L21.
 Bonsor A. and Wyatt M. (2010) *MNRAS*, 409, 1631.
 Bonsor A. and Wyatt M. C. (2012) *MNRAS*, 420, 2990.
 Bonsor A. et al. (2012) *AAp*, 548, A104.
 Bonsor A. et al. (2013a) *MNRAS*, 431, 3025.
 Bonsor A. et al. (2013b) *MNRAS*, 433, 2938.
 Booth M. et al. (2009) *MNRAS*, 399, 385.
 Booth M. et al. (2013) *MNRAS*, 428, 1263.
 Brauer F. et al. (2008) *AAp*, 480, 859.
 Briggs R. E. (1962) *AJ*, 67, 710.
 Brinkworth C. S. et al. (2012) *ApJ*, 750, 86.
 Broekhoven-Fiene H. et al. (2013) *ApJ*, 762, 52.
 Bryden G. et al. (2009) *ApJ*, 705, 1226.
 Bryden et al. (2013) *ApJ*, in preparation.
 Buenzli E. et al. (2010) *AAp*, 524, L1.
 Campo Bagatin A. et al. (1994) *PSS*, 42, 1079.
 Capobianco C. C. et al. (2011) *Icarus*, 211, 819.
 Carpenter J. M. et al. (2009) *ApJS*, 181, 197.
 Chen C. H. et al. (2006) *ApJS*, 166, 351.
 Chen C. H. et al. (2007) *ApJ*, 666, 466.
 Chen C. H. et al. (2008) *ApJ*, 689, 539.
 Chen C. H. et al. (2011) *ApJ*, 738, 122.
 Chen C. H. et al. (2012) *ApJ*, 756, 133.
 Chiang E. and Youdin A. N. (2010) *ARvEPS*, 38, 493.
 Chiang E. et al. (2009) *ApJ*, 693, 734.
 Churcher L. J. et al. (2011) *MNRAS*, 417, 1715.
 Clampin M. et al. (2003) *AJ*, 126, 385.
 Cranmer S. R. et al. (2013) *ApJ*, 772, 149.
 Czechowski A. and Mann I. (2007) *ApJ*, 660, 1541.
 Davies M. et al. (2014) *Protostars and Planets VI*, in press.
 Dawson R. I. et al. (2012) *ApJ*, 761, 163.
 de Vries B. L. et al. (2012) *Nature*, 490, 74.
 Debes J. H. et al. (2009) *ApJ*, 702, 318.
 Deller A. T. and Maddison S. T. (2005) *ApJ*, 625, 398.
 Dent W. et al. (2013) *Science*, submitted.
 di Folco E. et al. (2004) *AAp*, 426, 601.
 di Folco E. et al. (2007) *AAp*, 475, 243.
 Dodson-Robinson S. E. et al. (2009) *Icarus*, 200, 672.
 Dodson-Robinson S. E. et al. (2011) *AJ*, 141, 11.
 Dohnanyi J. S. (1969) *JGR*, 74, 2531.
 Dominik C. and Decin G. (2003) *ApJ*, 598, 626.
 Donaldson J. K. et al. (2013) *ApJ*, 772, 17.
 Dong R. et al. (2010) *ApJ*, 715, 1036.
 Dufour P. et al. (2012) *ApJ*, 749, 6.
 Dukes D. and Krumholz M. R. (2012) *ApJ*, 754, 56.
 Dunham M. M. et al. (2014) *Protostars and Planets VI*, in press.
 Durda D. D. and Dermott S. F. (1997) *Icarus*, 130, 140.
 Dutrey A. et al. (2014) *Protostars and Planets VI*, in press.
 Eiroa C. et al. (2010) *AAp*, 518, L131.
 Eiroa C. et al. (2011) *AAp*, 536, L4.
 Eiroa C. et al. (2013) *AAp*, 555, A11.
 Endl M. et al. (2008) *ApJ*, 673, 1165.
 Ertel et al. (2013) *AAp*, in preparation.
 Espaillat C. et al. (2014) *Protostars and Planets VI*, in press.
 Faber P. and Quillen A. C. (2007) *MNRAS*, 382, 1823.
 Ferlet R. et al. (1987) *AAp*, 185, 267.
 Fernandez J. A. and Ip W.-H. (1984) *Icarus*, 58, 109.
 Fernández R. et al. (2006) *ApJ*, 643, 509.
 Forbrich J. et al. (2008) *ApJ*, 687, 1107.
 Fujiwara H. et al. (2009) *ApJL*, 695, L88.
 Fujiwara H. et al. (2012) *ApJ*, 749, L29.
 Gänsicke B. T. et al. (2008) *MNRAS*, 391, L103.
 Gáspár A. et al. (2008) *ApJ*, 672, 974.
 Gáspár A. et al. (2013) *ApJ*, 768, 25.
 Gautier III T. N. et al. (2007) *ApJ*, 667, 527.
 Girven J. et al. (2011) *MNRAS*, 417, 1210.
 Golimowski D. A. et al. (2006) *AJ*, 131, 3109.
 Gomes R. et al. (2005) *Nature*, 435, 466.
 Gomes R. S. et al. (2004) *Icarus*, 170, 492.
 Gorlova N. et al. (2006) *ApJ*, 649, 1028.
 Graham J. R. et al. (1990) *ApJ*, 357, 216.
 Graham J. R. et al. (2007) *ApJ*, 654, 595.

- Greaves J. S. et al. (1998) *ApJL*, 506, L133.
- Greaves J. S. et al. (2005) *ApJL*, 619, L187.
- Greaves J. S. et al. (2006) *MNRAS*, 366, 283.
- Greaves J. S. et al. (2013) *MNRAS*, in press.
- Grigorieva A. et al. (2007) *AAP*, 461, 537.
- Güttler C. et al. (2010) *AAP*, 513, A56.
- Habing H. J. et al. (2001) *AAP*, 365, 545.
- Haisch K. E. et al. (2001) *ApJL*, 553, L153.
- Heap S. R. et al. (2000) *ApJ*, 539, 435.
- Heng K. and Malik M. (2013) *MNRAS*, 432, 2562.
- Heng K. and Tremaine S. (2010) *MNRAS*, 401, 867.
- Hernández J. et al. (2007) *ApJ*, 662, 1067.
- Hillenbrand L. A. (2008) *Physica Scripta Volume T*, 130, 1, 014024.
- Hillenbrand L. A. et al. (2008) *ApJ*, 677, 630.
- Hines D. C. et al. (2007) *ApJL*, 671, L165.
- Hinkley S. et al. (2009) *ApJ*, 701, 804.
- Hinz P. M. et al. (2008) in: *SPIE Conf. Ser.*, vol. 7013.
- Hobbs L. M. et al. (1985) *ApJL*, 293, L29.
- Holland W. S. et al. (1998) in: *Advanced Technology MMW, Radio, and Terahertz Telescopes*, vol. 3357 of *Society of Photo-Optical Instrumentation Engineers (SPIE) Conference Series*, (edited by T. G. Phillips), pp. 305–318.
- Hughes A. M. et al. (2008a) *ApJ*, 681, 626.
- Hughes A. M. et al. (2008b) *ApJ*, 678, 1119.
- Hughes A. M. et al. (2012) *ApJ*, 750, 82.
- Jackson A. P. and Wyatt M. C. (2012) *MNRAS*, 425, 657.
- Janson M. et al. (2013) *ApJ*, 773, 73.
- Jolly A. et al. (1998) *AAP*, 329, 1028.
- Kains N. et al. (2011) *MNRAS*, 414, 2486.
- Kalas P. et al. (2005) *Nature*, 435, 1067.
- Kalas P. et al. (2007) *ApJL*, 661, L85.
- Kalas P. et al. (2008) *Science*, 322, 1345.
- Kalas P. et al. (2013) *ApJ*, 775, 56.
- Kelsall T. et al. (1998) *ApJ*, 508, 44.
- Kennedy G. M. and Wyatt M. C. (2010) *MNRAS*, 405, 1253.
- Kennedy G. M. and Wyatt M. C. (2011) *MNRAS*, 412, 2137.
- Kennedy G. M. and Wyatt M. C. (2012) *MNRAS*, 426, 91.
- Kennedy G. M. and Wyatt M. C. (2013) *MNRAS*, 433, 2334.
- Kennedy G. M. et al. (2012a) *MNRAS*, 421, 2264.
- Kennedy G. M. et al. (2012b) *MNRAS*, 426, 2115.
- Kennedy G. M. et al. (2013a) *MNRAS*, in press.
- Kennedy G. M. et al. (2013b) *MNRAS*, 436, 898.
- Kenyon S. J. and Bromley B. C. (2002) *AJ*, 123, 1757.
- Kenyon S. J. and Bromley B. C. (2004) *ApJL*, 602, L133.
- Kenyon S. J. and Bromley B. C. (2005) *AJ*, 130, 269.
- Kenyon S. J. and Bromley B. C. (2008) *ApJS*, 179, 451.
- Kenyon S. J. and Bromley B. C. (2010) *ApJS*, 188, 242.
- Kilias E. et al. (2013) *ApJ*, in preparation.
- Kilic M. and Redfield S. (2007) *ApJ*, 660, 641.
- Kilic M. et al. (2005) *ApJL*, 632, L115.
- Kilic M. et al. (2006) *ApJ*, 646, 474.
- Kilic M. et al. (2009) *ApJ*, 696, 2094.
- Kirsh D. R. et al. (2009) *Icarus*, 199, 197.
- Klahr H. and Lin D. N. C. (2005) *ApJ*, 632, 1113.
- Kobayashi H. and Ida S. (2001) *Icarus*, 153, 416.
- Kobayashi H. et al. (2008) *Icarus*, 195, 871.
- Koerner D. W. et al. (2010) *ApJL*, 710, L26.
- Kóspál Á. et al. (2009) *ApJL*, 700, L73.
- Kóspál Á. et al. (2013) *ApJ*, 776, 77.
- Kozai Y. (1962) *AJ*, 67, 591.
- Kral Q. et al. (2013) *AAP*, 558, A121.
- Krist J. E. et al. (2012) *AJ*, 144, 45.
- Krivov A. V. (2010) *RAA*, 10, 383.
- Krivov A. V. et al. (2000) *AAP*, 362, 1127.
- Krivov A. V. et al. (2005) *Icarus*, 174, 105.
- Krivov A. V. et al. (2006) *AAP*, 455, 509.
- Krivov A. V. et al. (2007) *AAP*, 462, 199.
- Krivov A. V. et al. (2008) *ApJ*, 687, 608.
- Krivov A. V. et al. (2009) *AAP*, 507, 1503.
- Krivov A. V. et al. (2013) *ApJ*, 772, 32.
- Kroupa P. (1995) *MNRAS*, 277, 1507.
- Kroupa P. (1998) *MNRAS*, 298, 231.
- Kuchner M. J. and Holman M. J. (2003) *ApJ*, 588, 1110.
- Kuchner M. J. and Stark C. C. (2010) *AJ*, 140, 1007.
- Lagrange A. et al. (2010) *Science*, 329, 57.
- Lagrange A.-M. et al. (2009) *AAP*, 493, L21.
- Lagrange A.-M. et al. (2012) *AAP*, 542, A40.
- Lawler S. M. et al. (2009) *ApJ*, 705, 89.
- Lebreton J. et al. (2012) *AAP*, 539, A17.
- Lecar M. et al. (2001) *ARAA*, 39, 581.
- Lecar M. et al. (2006) *ApJ*, 640, 1115.
- Lecavelier des Etangs A. et al. (1996a) *AAP*, 307, 542.
- Lecavelier des Etangs A. et al. (1996b) *Icarus*, 123, 168.
- Lecavelier des Etangs A. et al. (1998) *AAP*, 339, 477.
- Lecavelier des Etangs A. et al. (2001) *Nature*, 412, 706.
- Lestrade J.-F. et al. (2006) *AAP*, 460, 733.
- Lestrade J.-F. et al. (2012) *AAP*, 548, A86.
- Levison H. F. and Duncan M. J. (1997) *Icarus*, 127, 13.
- Levison H. F. et al. (2007) *Protostars and Planets V*, pp. 669–684.
- Li D. et al. (2012) *ApJ*, 759, 81.
- Li Z. et al. (2014) *Protostars and Planets VI*, in press.
- Lisse C. M. et al. (2008) *ApJ*, 673, 1106.
- Lisse C. M. et al. (2009) *ApJ*, 701, 2019.
- Lisse C. M. et al. (2012) *ApJ*, 747, 93.
- Löhne T. et al. (2008) *ApJ*, 673, 1123.
- Löhne T. et al. (2012) *AAP*, 537, A110.
- Low F. J. et al. (1984) *ApJL*, 278, L19.
- Low F. J. et al. (2005) *ApJ*, 631, 1170.
- Lyra W. and Kuchner M. J. (2013) *Nature*, 499, 184.
- MacGregor M. A. et al. (2013) *ApJL*, 762, L21.
- Maldonado J. et al. (2012) *AAP*, 541, A40.
- Malhotra R. (1993) *Nature*, 365, 819.
- Maness H. L. et al. (2008) *ApJL*, 686, L25.
- Maness H. L. et al. (2009) *ApJ*, 707, 1098.
- Marois C. et al. (2008) *Science*, 322, 1348.
- Marois C. et al. (2010) *Nature*, 468, 1080.
- Marshall J. P. et al. (2011) *AAP*, 529, A117.
- Marshall et al. (2013) *ApJ*, submitted.
- Marzari F. and Thébault P. (2011) *MNRAS*, 416, 1890.
- Marzari F. et al. (2012) *AAP*, 539, A98.
- Matthews B. C. et al. (2007) *ApJ*, 663, 1103.
- Matthews B. C. et al. (2010) *AAP*, 518, L135.
- Matthews B. C. et al. (2013a) *ArXiv e-prints*.
- Matthews B. C. et al. (2013b) *MNRAS*, in preparation.
- Melis C. et al. (2010) *ApJL*, 717, L57.
- Melis C. et al. (2012) *Nature*, 487, 74.
- Meng H. Y. A. et al. (2012) *ApJL*, 751, L17.
- Metzger B. D. et al. (2012) *MNRAS*, 423, 505.
- Meyer M. R. et al. (2006) *PASP*, 118, 1690.
- Meyer M. R. et al. (2007) *Protostars and Planets V*, pp. 573–588.
- Millan-Gabet R. et al. (2011) *ApJ*, 734, 67.
- Moerchen M. M. et al. (2010) *ApJ*, 723, 1418.
- Monin J.-L. et al. (2007) *Protostars and Planets V*, pp. 395–409.

- Moór A. et al. (2011a) *ApJL*, 740, L7.
- Moór A. et al. (2011b) *ApJS*, 193, 4.
- Moore A. and Quillen A. C. (2013) *MNRAS*, 430, 320.
- Morales F. Y. et al. (2009) *ApJ*, 699, 1067.
- Morales F. Y. et al. (2011) *ApJL*, 730, L29.
- Morbidelli A. et al. (2004) *MNRAS*, 355, 935.
- Moro-Martín A. et al. (2010) *ApJ*, 717, 1123.
- Moro-Martín et al. (2013) *ApJ*, in prep.
- Mouillet D. et al. (1997) *MNRAS*, 292, 896.
- Müller S. et al. (2010) *ApJ*, 708, 1728.
- Murray C. D. and Dermott S. F. (1999) *Solar system dynamics*.
- Mustill A. J. and Wyatt M. C. (2009) *MNRAS*, 399, 1403.
- Mustill A. J. and Wyatt M. C. (2011) *MNRAS*, 413, 554.
- Mustill A. J. and Wyatt M. C. (2012) *MNRAS*, 419, 3074.
- Najita J. and Williams J. P. (2005) *ApJ*, 635, 625.
- Nesvold E. R. et al. (2013) *ApJ*, 777, 144.
- Nesvorný D. et al. (2003) *ApJ*, 591, 486.
- Nesvorný D. et al. (2010) *ApJ*, 713, 816.
- Nilsson R. et al. (2010) *AAp*, 518, A40.
- O'Brien D. P. and Greenberg R. (2003) *Icarus*, 164, 334.
- Olofsson G. et al. (2001) *ApJ*, 563, L77.
- Ozernoy L. M. et al. (2000) *ApJL*, 537, L147.
- Pan M. and Schlichting H. E. (2012) *ApJ*, 747, 113.
- Panić O. et al. (2013) *MNRAS*, 435, 1037.
- Pascucci I. et al. (2006) *ApJ*, 651, 1177.
- Payne M. J. et al. (2009) *MNRAS*, 393, 1219.
- Phillips N. et al. (2013) *MNRAS*, in preparation.
- Plavchan P. et al. (2005) *ApJ*, 631, 1161.
- Plavchan P. et al. (2009) *ApJ*, 698, 1068.
- Pontoppidan K. et al. (2014) *Protostars and Planets VI*, in press.
- Poulton C. J. et al. (2006) *MNRAS*, 372, 53.
- Quillen A. C. (2006) *MNRAS*, 372, L14.
- Quillen A. C. and Thorndike S. (2002) *ApJ*, 578, L149.
- Rafikov R. R. (2011a) *ApJL*, 732, L3.
- Rafikov R. R. (2011b) *MNRAS*, 416, L55.
- Raymond S. et al. (2014) *Protostars and Planets VI*, in press.
- Raymond S. N. and Armitage P. J. (2013) *MNRAS*, 429, L99.
- Raymond S. N. et al. (2012) *AAp*, 541, A11.
- Reche R. et al. (2008) *AAp*, 480, 551.
- Reidemeister M. et al. (2009) *AAp*, 503, 247.
- Reidemeister M. et al. (2011) *AAp*, 527, A57.
- Rhee J. H. et al. (2007) *ApJ*, 660, 1556.
- Rhee J. H. et al. (2008) *ApJ*, 675, 777.
- Rieke G. H. et al. (2005) *ApJ*, 620, 1010.
- Rivera E. J. et al. (2005) *ApJ*, 634, 625.
- Riviere-Marichalar P. et al. (2013) *AAp*, 555, A67.
- Roberge A. et al. (2000) *ApJ*, 538, 904.
- Roberge A. et al. (2006) *Nature*, 441, 724.
- Roberge A. et al. (2012) *PASP*, 124, 799.
- Roberge A. et al. (2013) *ApJ*, 771, 69.
- Roccatagliata V. et al. (2009) *AAp*, 497, 409.
- Rodigas T. J. et al. (2012) *ApJ*, 752, 57.
- Rodriguez D. et al. (2013) *MNRAS*, in preparation.
- Rodriguez D. R. and Zuckerman B. (2012) *ApJ*, 745, 147.
- Rosenfeld K. A. et al. (2012) *ApJ*, 757, 129.
- Schneider G. et al. (1999) *ApJL*, 513, L127.
- Schneider G. et al. (2005) *ApJL*, 629, L117.
- Shen Y. et al. (2009) *ApJ*, 696, 2126.
- Sibthorpe B. et al. (2010) *AAp*, 518, L130.
- Sibthorpe B. et al. (2013) *MNRAS*, in preparation.
- Siegler N. et al. (2007) *ApJ*, 654, 580.
- Slettebak A. (1975) *ApJ*, 197, 137.
- Smith B. A. and Terrile R. J. (1984) *Science*, 226, 1421.
- Smith R. et al. (2009) *AAp*, 503, 265.
- Smith R. et al. (2012) *MNRAS*, 422, 2560.
- Song I. et al. (2005) *Nature*, 436, 363.
- Stapelfeldt K. R. et al. (2004) *ApJ*, 154, 458.
- Stark C. C. and Kuchner M. J. (2009) *ApJ*, 707, 543.
- Stencel R. E. and Backman D. E. (1991) *ApJS*, 75, 905.
- Strubbe L. E. and Chiang E. I. (2006) *ApJ*, 648, 652.
- Su K. Y. L. et al. (2005) *ApJ*, 628, 487.
- Su K. Y. L. et al. (2006) *ApJ*, 653, 675.
- Su K. Y. L. et al. (2007) *ApJL*, 657, L41.
- Su K. Y. L. et al. (2009) *ApJ*, 705, 314.
- Su K. Y. L. et al. (2013) *ApJ*, 763, 118.
- Takeuchi T. and Artymowicz P. (2001) *ApJ*, 557, 990.
- Telesco C. M. et al. (2000) *ApJ*, 530, 329.
- Thébault P. and Augereau J.-C. (2005) *AAp*, 437, 141.
- Thébault P. and Augereau J.-C. (2007) *AAp*, 472, 169.
- Thébault P. and Wu Y. (2008) *AAp*, 481, 713.
- Thalmann C. et al. (2011) *ApJL*, 743, L6.
- Thébault P. (2009) *AAp*, 505, 1269.
- Thébault P. (2012) *AAp*, 537, A65.
- Thébault P. et al. (2003) *AAp*, 408, 775.
- Thébault P. et al. (2010) *AAp*, 524, A13.
- Thébault P. et al. (2012) *AAp*, 547, A92.
- Thureau N. et al. (2013) *MNRAS*, in preparation.
- Tielens A. G. G. M. et al. (1994) *ApJ*, 431, 321.
- Trilling D. E. et al. (2007) *ApJ*, 658, 1289.
- Trilling D. E. et al. (2008) *ApJ*, 674, 1086.
- Udry S. et al. (2007) *AAp*, 469, L43.
- Urban L. E. et al. (2012) *ApJ*, 750, 98.
- van Dishoeck E. F. and Black J. H. (1988) *ApJ*, 334, 771.
- Vidal-Madjar A. et al. (1994) *AAp*, 290, 245.
- Vitense C. et al. (2012) *AAp*, 540, A30.
- Watson C. A. et al. (2011) *MNRAS*, 413, L71.
- Weidenschilling S. J. (1977) *MNRAS*, 180, 57.
- Weidenschilling S. J. and Jackson A. A. (1993) *Icarus*, 104, 244.
- Weinberger A. J. et al. (2011) *ApJ*, 726, 72.
- Wilner D. J. et al. (2012) *ApJL*, 749, L27.
- Wisdom J. (1980) *AJ*, 85, 1122.
- Wyatt M. C. (2003) *ApJ*, 598, 1321.
- Wyatt M. C. (2005a) *AAp*, 440, 937.
- Wyatt M. C. (2005b) *AAp*, 433, 1007.
- Wyatt M. C. (2006) *ApJ*, 639, 1153.
- Wyatt M. C. (2008) *ARAA*, 46, 339.
- Wyatt M. C. and Dent W. R. F. (2002) *MNRAS*, 334, 589.
- Wyatt M. C. et al. (1999) *ApJ*, 527, 918.
- Wyatt M. C. et al. (1999) *ApJ*, 527, 918.
- Wyatt M. C. et al. (2005) *ApJ*, 620, 492.
- Wyatt M. C. et al. (2007a) *MNRAS*, 380, 1737.
- Wyatt M. C. et al. (2007b) *ApJ*, 663, 365.
- Wyatt M. C. et al. (2007c) *ApJ*, 658, 569.
- Wyatt M. C. et al. (2010) *MNRAS*, 402, 657.
- Wyatt M. C. et al. (2011) *CMDA*, 111, 1.
- Wyatt M. C. et al. (2012) *MNRAS*, 424, 1206.
- Zsom A. et al. (2010) *AAp*, 513, A57.
- Zsom A. et al. (2011) *AAp*, 534, A73.
- Zuckerman B. and Becklin E. E. (1987) *Nature*, 330, 138.
- Zuckerman B. and Song I. (2004) *ARAA*, 42, 685.
- Zuckerman B. and Song I. (2012) *ApJ*, 758, 77.
- Zuckerman B. et al. (2001) *ApJL*, 562, L87.
- Zuckerman B. et al. (2003) *ApJ*, 596, 477.

